REFERENCE USE ONLY

REPORT NO. DOT-TSC-OST-75-26.III

LEAN MIXTURE ENGINES TESTING AND EVALUATION PROGRAM

Volume III: Appendices

Mack W. Dowdy
Frank W. Hoehn
Tom G. Vanderbrug

NOVEMBER 1975

FINAL REPORT

DOCUMENT IS AVAILABLE TO THE PUBLIC THROUGH THE NATIONAL TECHNICAL INFORMATION SERVICE, SPRINGFIELD, VIRGINIA 22161

Prepared for

U.S. DEPARTMENT OF TRANSPORTATION

Office of the Secretary
Office of the Assistant Secretary for
Systems Development and Technology
Office of Systems Engineering
Washington DC 20590

NOTICE

This document is disseminated under the sponsorship of the Department of Transportation in the interest of information exchange. The United States Government assumes no liability for its contents or use thereof.

NOTICE

The United States Government does not endorse products or manufacturers. Trade or manufacturers' names appear herein solely because they are considered essential to the object of this report.

Technical Report Documentation Page

1. Report No.	2. Government Accession No.	3. Recipient's Catalog No.
DOT-TSC-OST-75-26. III		

4. Title and Subtitle	5. Report Date
LEAN MIXTURE ENGINES TESTING AND EVALUATION PROGRAM Volume III: Appendices	November 1975
	6. Performing Organization Code
7. Author(s) Mack W. Dowdy, Frank W. Hoehn and Tom G. Vanderbrug	8. Performing Organization Report No. JPL 5040-12, Vol. III DOT-TSC-OST-75-26. III
9. Performing Organization Name and Address Jet Propulsion Laboratory* 4800 Oak Grove Drive Pasadena, CA 91103	10. Work Unit No. (TRAIS) OS 614/R6506
	11. Contract or Grant No. RA 74-38 TMP-0223
12. Sponsoring Agency Name and Address U.S. Dept. of Transportation, Office of the Secretary, Office of the Assistant Secretary for Systems Development and Technology, Office of Systems Engineering, Washington, D.C. 20590	13. Type of Report and Period Covered Final Report May - Dec. 1974
	14. Sponsoring Agency Code

15. Supplementary Notes

*Under Contract to: U.S. Department of Transportation
Transportation Systems Center, Kendall Square
Cambridge, MA 02142

16. Abstract

This report is aimed at defining analytically and demonstrating experimentally the potential of the "lean-burn concept." Fuel consumption and emissions data are obtained on the engine dynamometer for the baseline engine, and two lean-burn configurations of the same engine and data comparisons are made. Individual cylinder equivalence ratios are measured to evaluate the cylinder-to-cylinder distribution. Pressure-time traces from individual cylinders are used to get information about ignition delay, combustion duration and cycle-to-cycle pressure variations. Fuel consumption and emissions data for one lean-burn configuration are obtained over the Federal Driving Cycle using a chassis dynamometer and the results are compared with the stock baseline results. Using experimental results and information from the existing literature, the potential of the "lean-burn concept" is assessed using the Blumberg-Kummer cycle analysis program.

17. Key Words	18. Distribution Statement
Automobiles Fuel Consumption Exhaust Emissions	Document is available to the public through the National Technical Information Service, Springfield, Virginia 22161

19. Security Classif. (of this report)	20. Security Classif. (of this page)	21. No. of Pages	22. Price
UNCLASSIFIED	UNCLASSIFIED	84	

Form DOT F 1700.7 (8-72) Reproduction of completed page authorized

PREFACE

The Appendices, which are included herein, present supplemental analysis methods, fuel economy and emissions test data, and a description of the instrumentation used in the lean mixture engines testing and evaluation program.

CONTENTS

APPENDICES

APPENDIX A

ANALYSIS METHODS

The following section briefly summarizes significant cycle methods and analysis methods for prediction of engine emissions and performance characteristics.

A.1 ENGINE PERFORMANCE

Ref.	Author	Description
25	Barton et al.	Model developed to relate gas velocity near the spark at time of ignition to initial burn duration and crank angle of maximum cylinder pressure. Model correlates cyclic dispersion with gas velocity variations. Requires estimate or measurement of chamber gas velocities.
13	Trayser et al.	Analysis of induction systems.
7	Yu, Henery T. C.	Prediction of mixture maldistribution effects on engine power and fuel economy.

A.2 FLAME THEORY AND COMBUSTION

27	Arrigoni et al.	Summarizes flame propagation theory and presents flame speed calculation methods.
45	Blizzard et al.	Excellent turbulent burning model for analysis of cylinder pressures, flame radii, and mass fractions burned. Although correlation formulas are required to determine turbulent eddy size and entrainment velocities, the model predicts flame propagation characteristics based on the combustion chamber aerodynamics and chemistry.
46	NASA Report 1300	Basic laminar and turbulent flame theory.
26	Winsor et al.	Analysis method to relate burn time combustion variations to local spark mixture motion or velocity variations.

A.3 HYDROCARBON EMISSIONS

47	Daniel, W. A.	Calculation of quench volume, based on method of Friedman and Johnston, with rough correlation to exhaust HC. Experimental data verifies quench distance formula.

Ref.	Author	Description
38	Daniel, W. A.	Presents a highly detailed, complete model of exhaust HC emissions. Requires knowledge or estimate of cylinder pressure-temperature history and empirical correlation with experimental data to determine many key variables. Includes effects of crevice volume, blowby, post-flame oxidation, residual fraction, and oxidation in exhaust.
35	Haskell et al.	Present simplified, straightforward method for calculation of top-land crevice volume produced HC emissions.
36	Wentworth, J. T.	Method for correlating average combustion chamber surface temperature to HC emissions.
A.4	NO_x EMISSIONS	
43	Blumberg et al.	Highly detailed model that allows variation of most engine parameters to study performance and emissions effects. Although crank angle of combustion interval is required as input, the model shows reasonable agreement with experimental data at A/F from 13.4 to 18.4.
48	Daneshyar et al.	A detailed description of the model is not presented, but reasonable values of NO_x emissions are obtained. The model has mixed and unmixed analysis options for calculation of combustion chamber temperature-pressure and combustion-emission history.
49	Komiyama et al.	Basically the same type of model developed by Blumberg (43), but reportedly improved in the areas of flame speed, ignition delya, and cycle-to-cycle pressure variation predictions. Although good agreement with experimental data is claimed, up to 30% error is shown with lean mixtures. (The authors attributed this discrepancy to errors in determining the average pressure-time curve.)
50	Lucas et al.	Stratified zone and mixed zone models are presented which generate cylinder pressure-temperature and exhaust NO_x formation data. The models include the effects of heat transfer, spark location, and exhaust valve location. The only input data specifically mentioned are an estimate of residual fraction and combustion chamber geometry. Good agreement with experimental data is shown except at lean mixtures (up to 50% error). The authors present several explanations for the lean mixture errors, however.

APPENDIX B

DATA FOR STOCK BASELINE

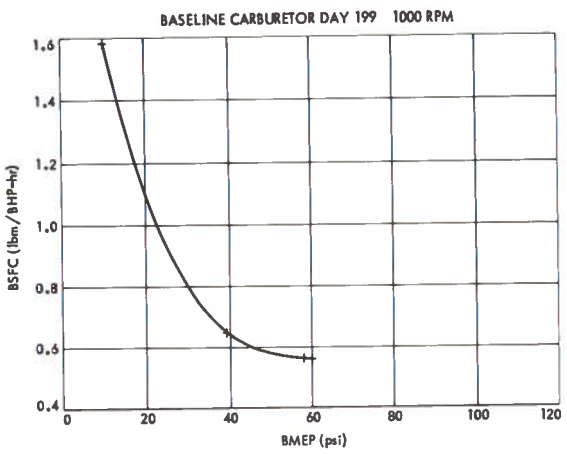

FIGURE B-1. BASELINE BSFC VERSUS BMEP FOR 1000 RPM

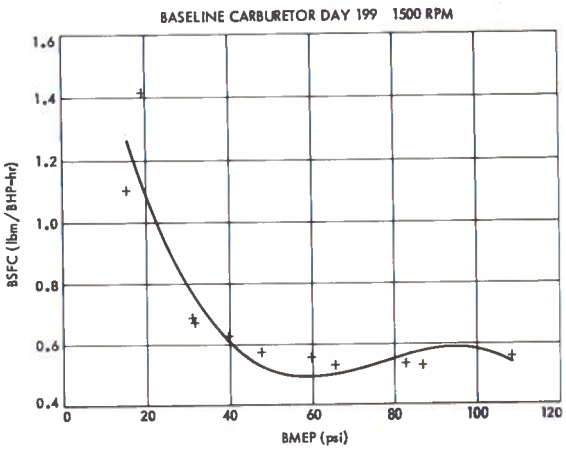

FIGURE B-2. BASELINE BSFC VERSUS BMEP FOR 1500 RPM

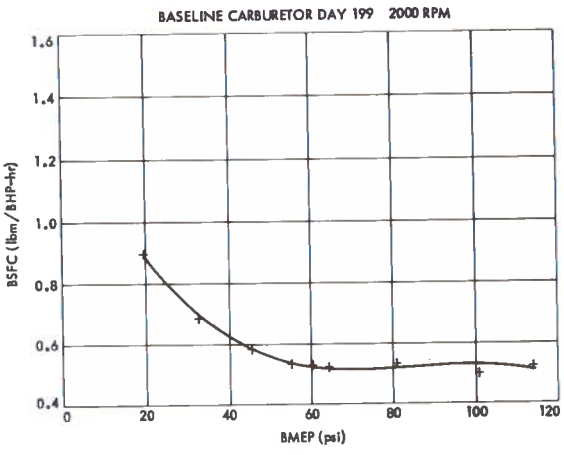

FIGURE B-3. BASELINE BSFC VERSUS BMEP FOR 2000 RPM

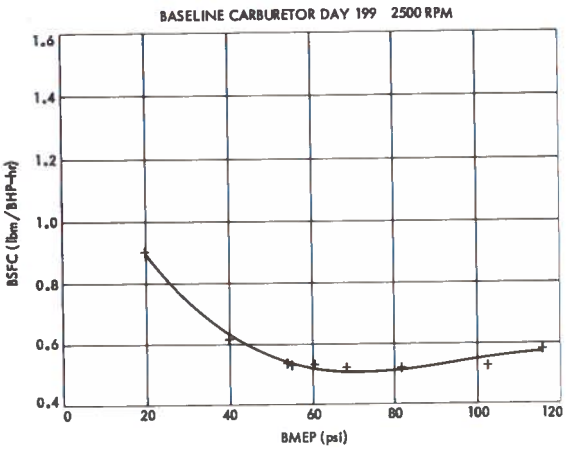

FIGURE B-4. BASELINE BSFC VERSUS BMEP FOR 2500 RPM

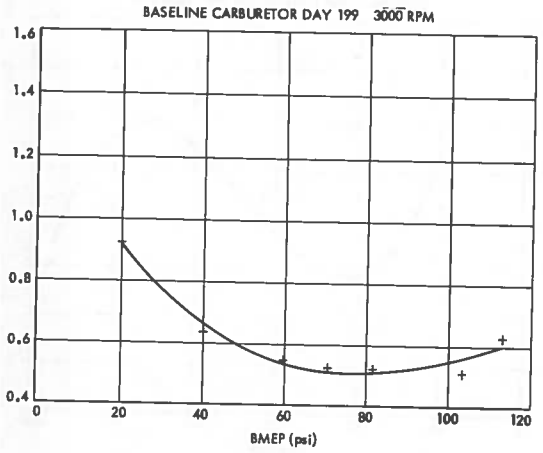

FIGURE B-5. BASELINE BSFC VERSUS BMEP FOR 3000 RPM

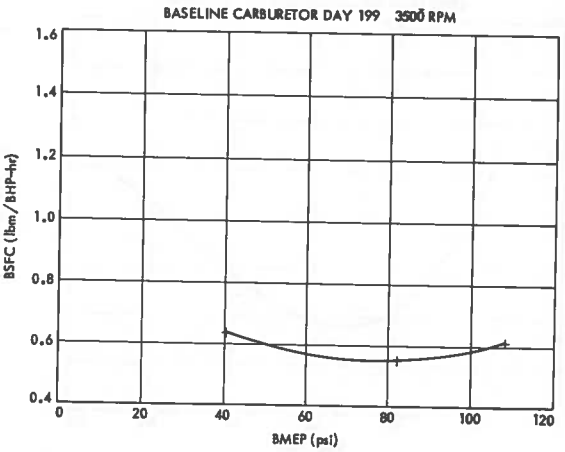

FIGURE B-6. BASELINE BSFC VERSUS BMEP FOR 3500 RPM

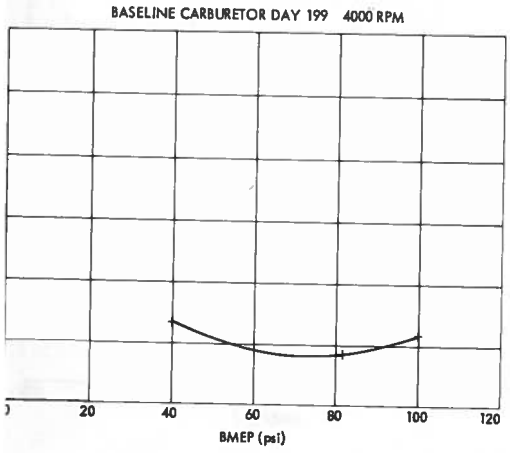

FIGURE B-7. BASELINE BSFC VERSUS BMEP FOR 4000 RPM

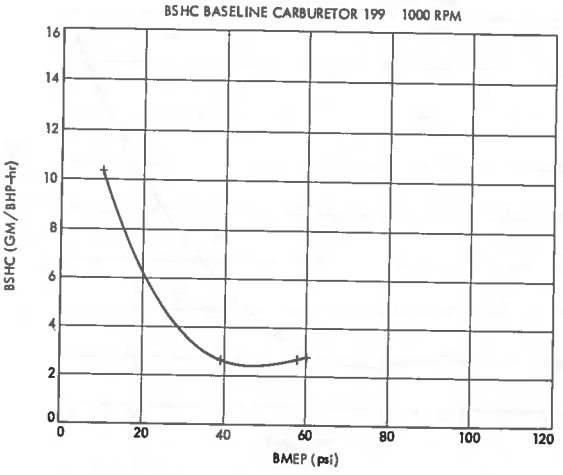

FIGURE B-8. BASELINE BSHC VERSUS BMEP FOR 1000 RPM

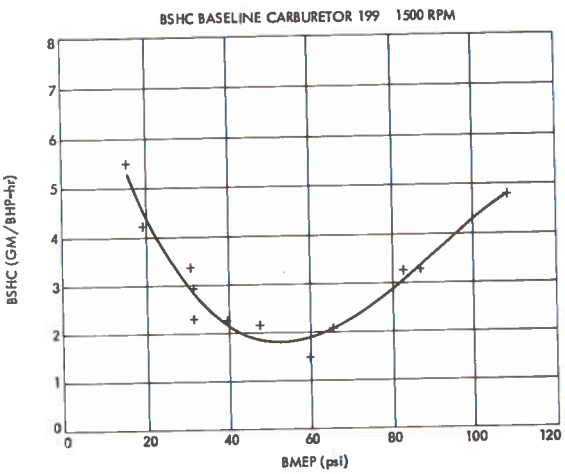

FIGURE B-9. BASELINE BSHC VERSUS BMEP FOR 1500 RPM

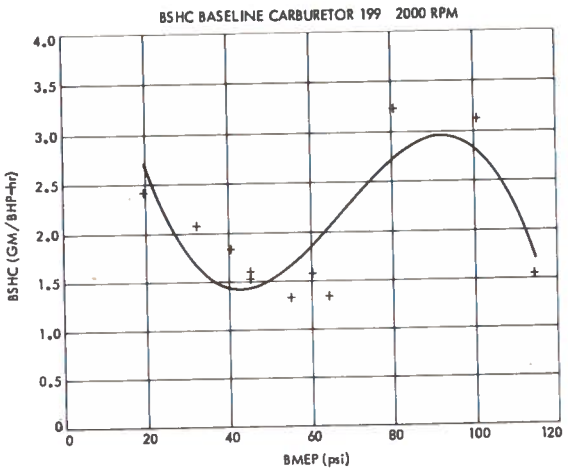

FIGURE B-10. BASELINE BSHC VERSUS BMEP FOR 2000 RPM

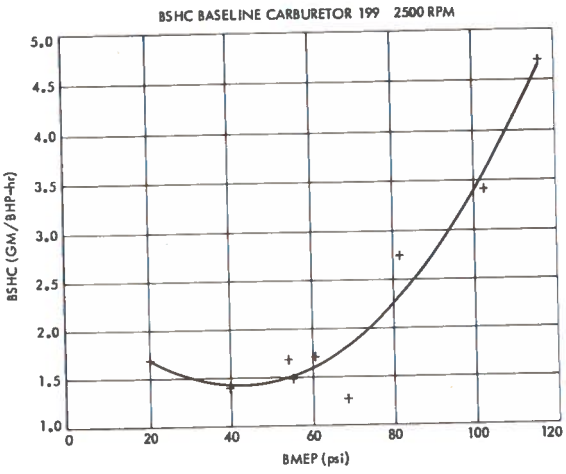

FIGURE B-11. BASELINE BSHC VERSUS BMEP FOR 2500 RPM

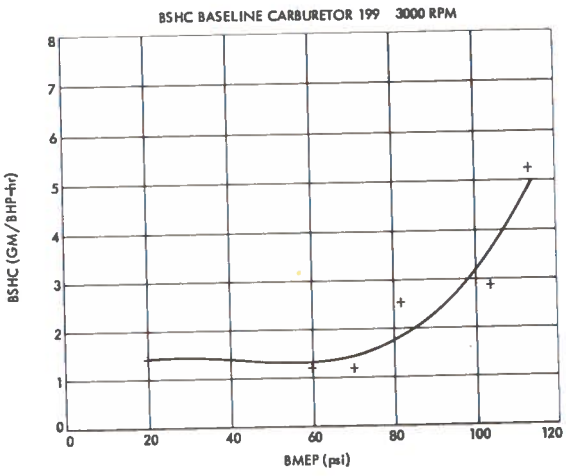

FIGURE B-12. BASELINE BSHC VERSUS BMEP FOR 3000 RPM

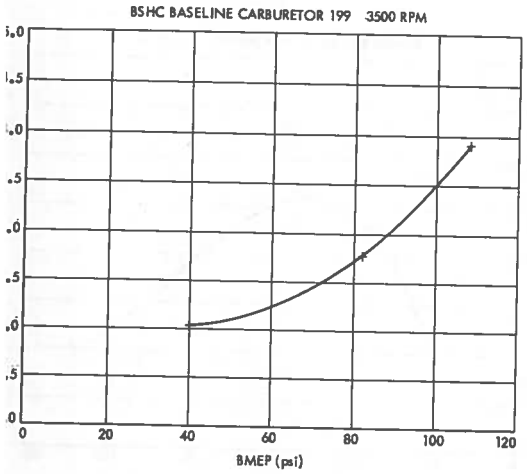

FIGURE B-13. BASELINE BSHC VERSUS BMEP FOR 3500 RPM

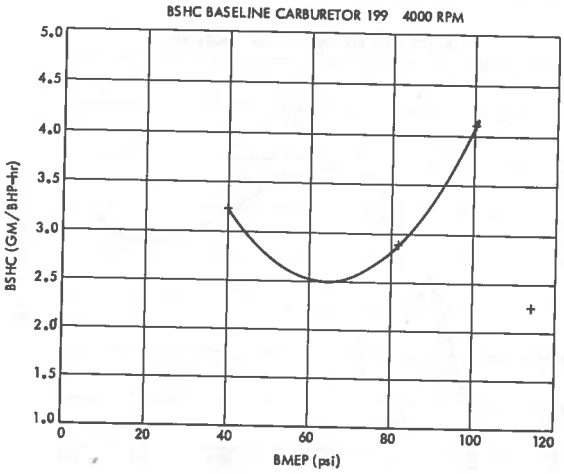

FIGURE B-14. BASELINE BSHC VERSUS BMEP FOR 4000 RPM

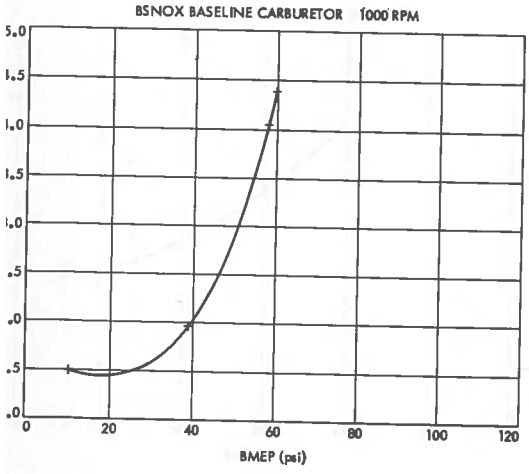

FIGURE B-15. BASELINE $BSNO_x$ VERSUS BMEP FOR 1000 RPM

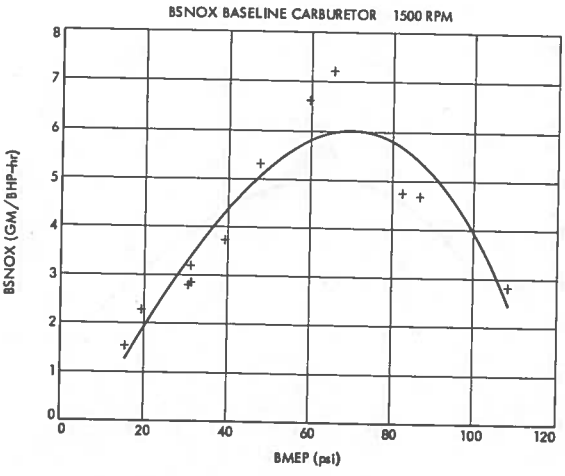

FIGURE B-16. BASELINE $BSNO_x$ VERSUS BMEP FOR 1500 RPM

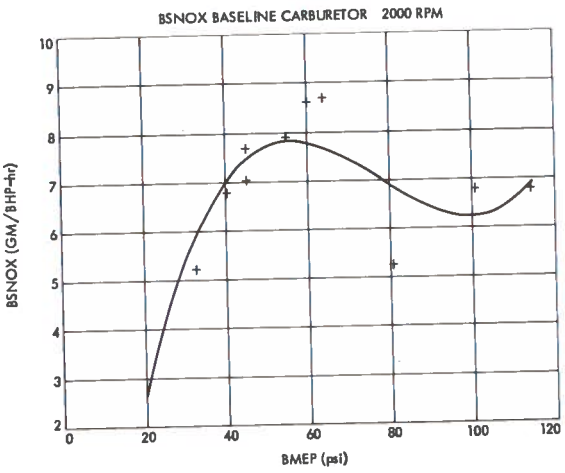

FIGURE B-17. BASELINE $BSNO_x$ VERSUS BMEP FOR 2000 RPM

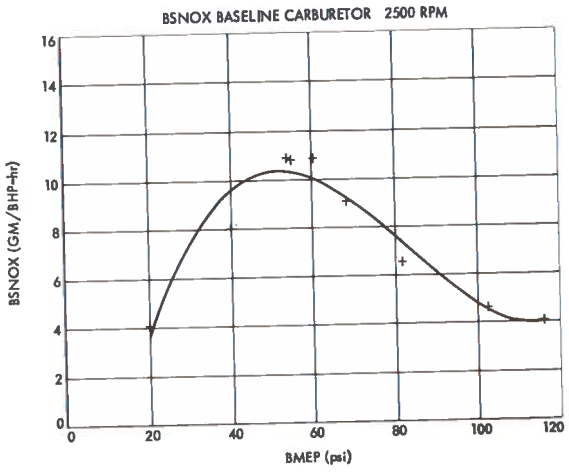

FIGURE B-18. BASELINE $BSNO_x$ VERSUS BMEP FOR 2500 RPM

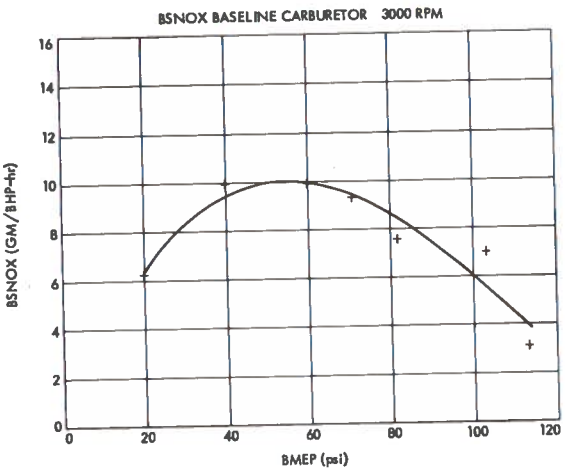

FIGURE B-19. BASELINE $BSNO_x$ VERSUS BMEP FOR 3000 RPM

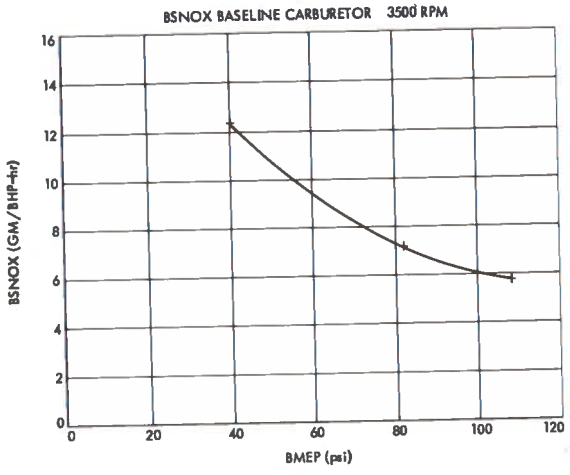

FIGURE B-20. BASELINE $BSNO_x$ VERSUS BMEP FOR 3500 RPM

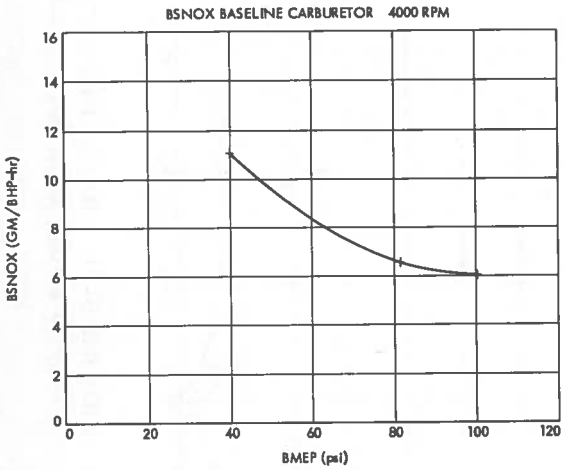

FIGURE B-21. BASELINE BSNO$_x$ VERSUS BMEP FOR 4000 RPM

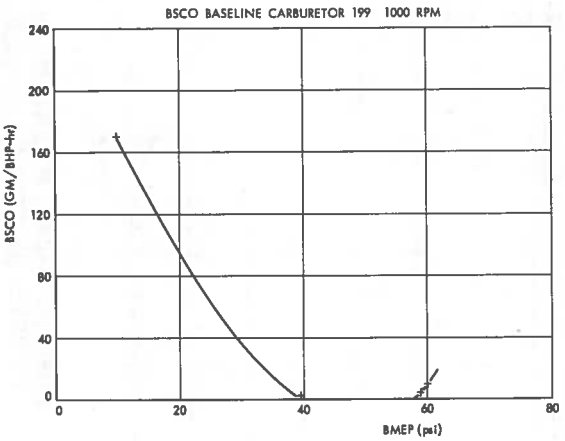

FIGURE B-22. BASELINE BSCO VERSUS BMEP FOR 1000 RPM

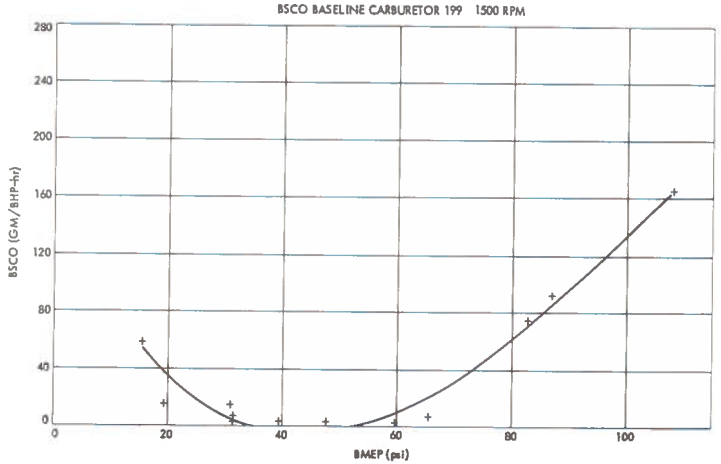

FIGURE B-23. BASELINE BSCO VERSUS BMEP FOR 1500 RPM

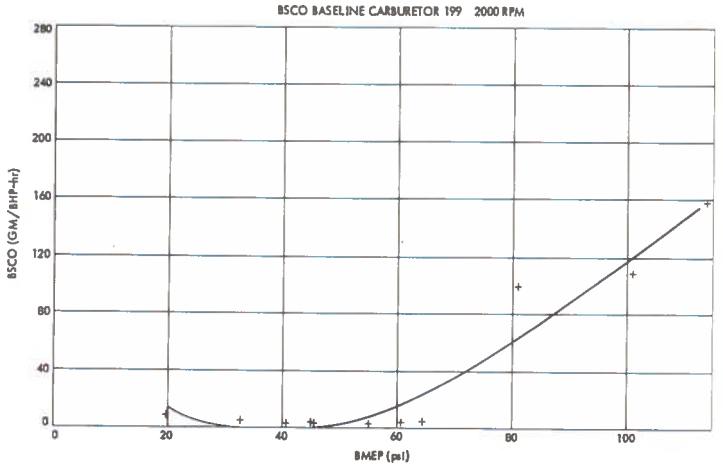

FIGURE B-24. BASELINE BSCO VERSUS BMEP FOR 2000 RPM

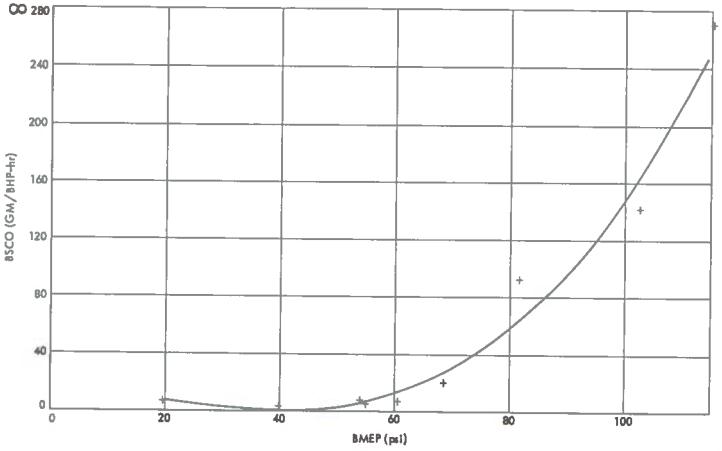

FIGURE B-25. BASELINE BSCO VERSUS BMEP FOR 2500 RPM

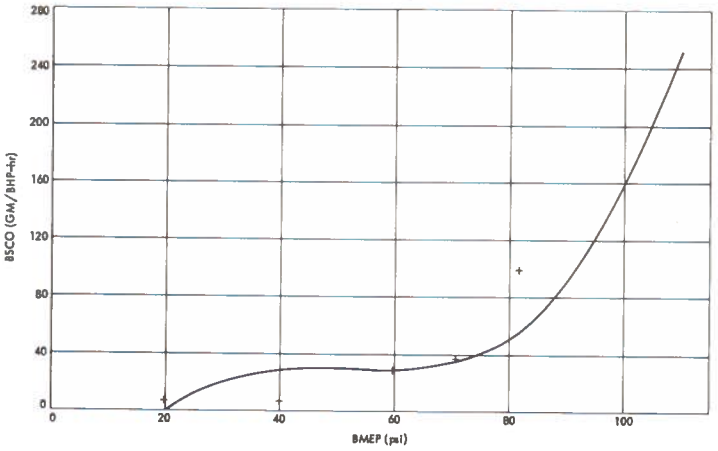

FIGURE B-26. BASELINE BSCO VERSUS BMEP FOR 3000 RPM

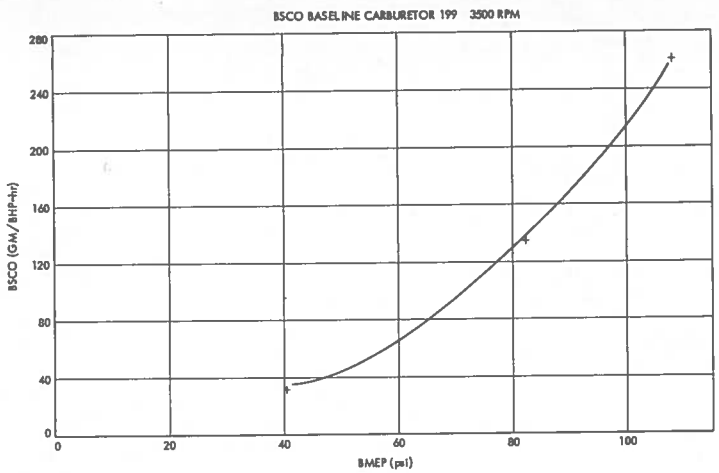

FIGURE B-27. BASELINE BSCO VERSUS BMEP FOR 3500 RPM

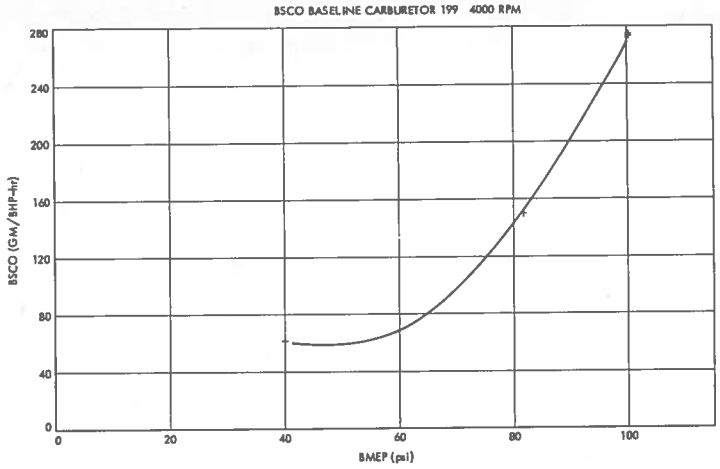

FIGURE B-28. BASELINE BSCO VERSUS BMEP FOR 4000 RPM

APPENDIX C

SENSITIVITY TEST DATA

FOR

LEAN BURN ENGINE CONFIGURATION No. 1

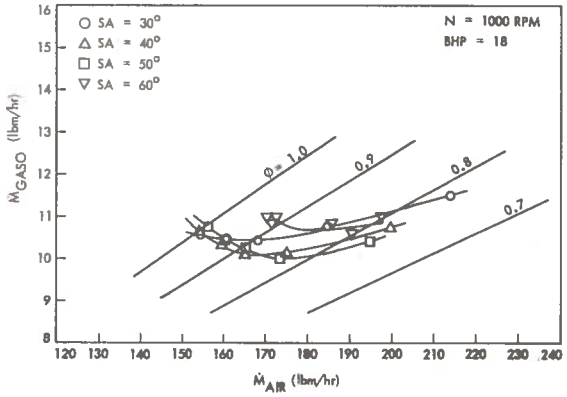

FIGURE C-1. FUEL CONSUMPTION CHARACTERISTIC (N=1000 RPM, BHP=18)

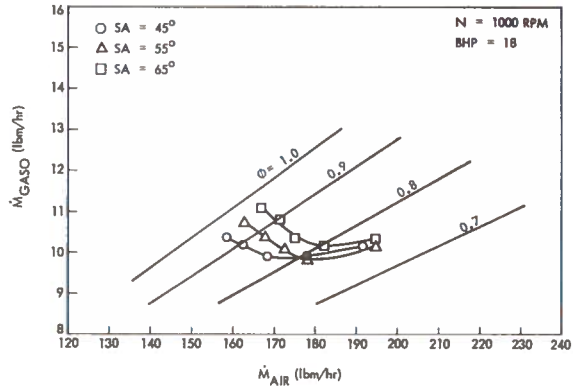

FIGURE C-2. FUEL CONSUMPTION CHARACTERISTIC (N=1000 RPM, BHP=18)

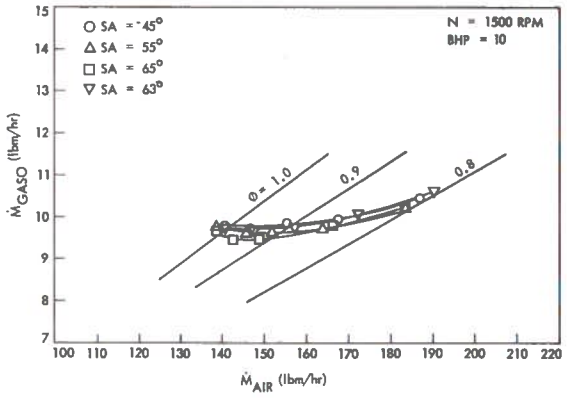

FIGURE C-3. FUEL CONSUMPTION CHARACTERISTIC (N=1500 RPM, BHP=10)

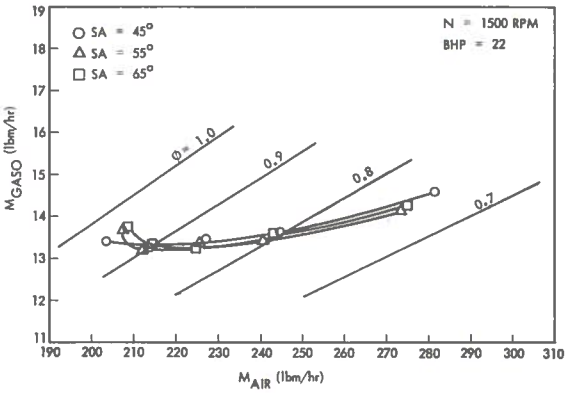

FIGURE C-4. FUEL CONSUMPTION CHARACTERISTIC (N=1500 RPM, BHP=22)

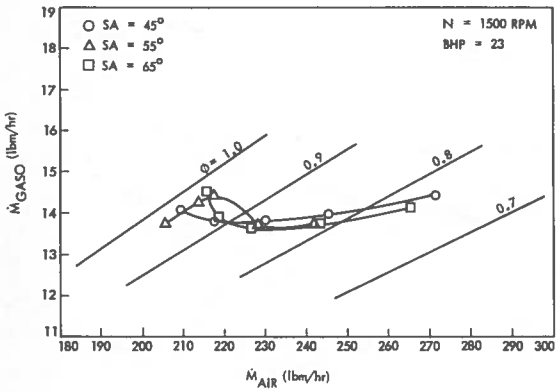

FIGURE C-5. FUEL CONSUMPTION CHARACTERISTIC (N=1500 RPM, BHP=23)

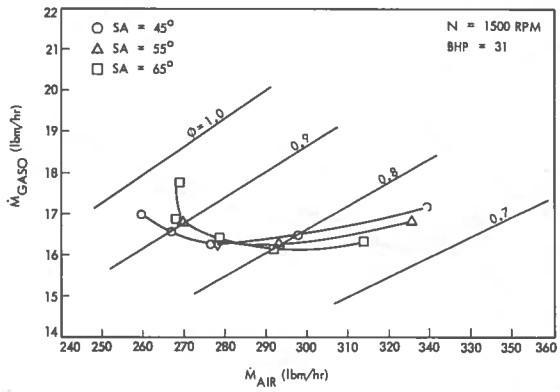

FIGURE C-6. FUEL CONSUMPTION CHARACTERISTIC (N=1500 RPM, BHP=31)

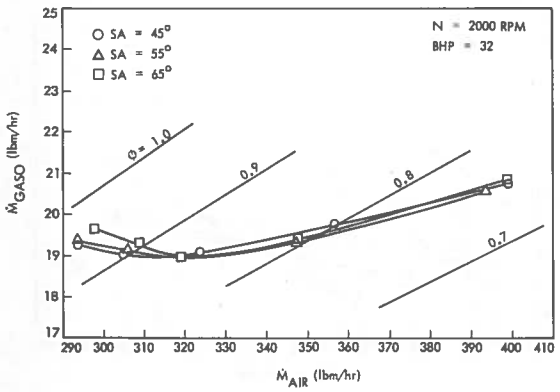

FIGURE C-7. FUEL CONSUMPTION CHARACTERISTIC (N=2000 RPM, BHP=32)

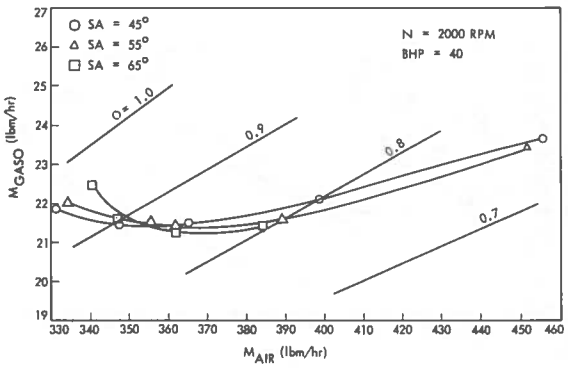

FIGURE C-8. FUEL CONSUMPTION CHARACTERISTIC (N=2000 RPM, BHP=40)

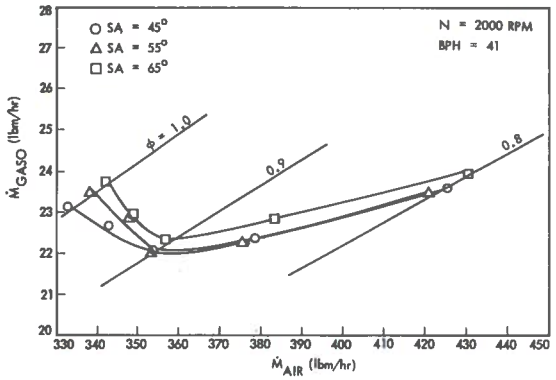

FIGURE C-9. FUEL CONSUMPTION CHARACTERISTIC (N=2000 RPM, BHP=41)

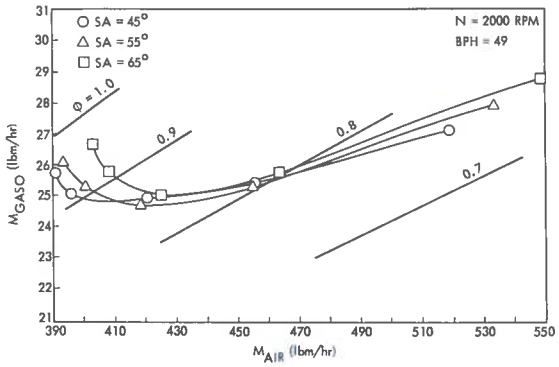

FIGURE C-10. FUEL CONSUMPTION CHARACTERISTIC (N=2000 RPM, BHP=49)

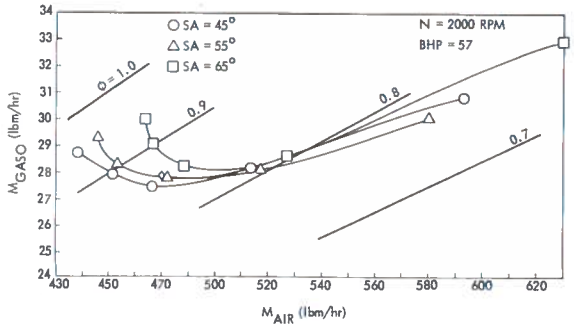

FIGURE C-11. FUEL CONSUMPTION CHARACTERISTIC (N=2000 RPM, BHP=57)

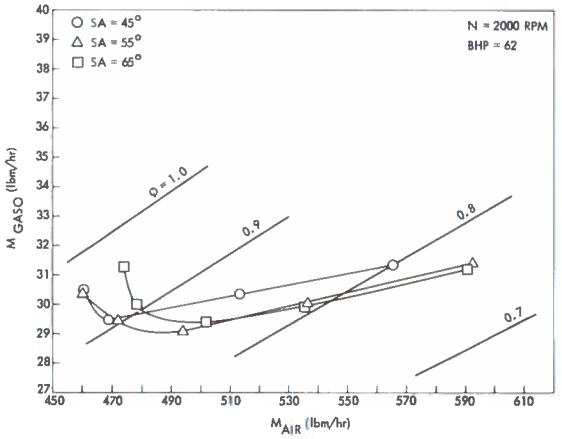

FIGURE C-12. FUEL CONSUMPTION CHARACTERISTIC (N=2000 RPM, BHP=62)

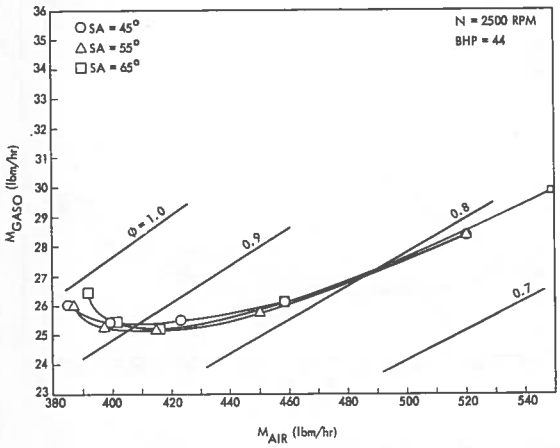

FIGURE C-13. FUEL CONSUMPTION CHARACTERISTIC (N=2500 RPM, BHP=44)

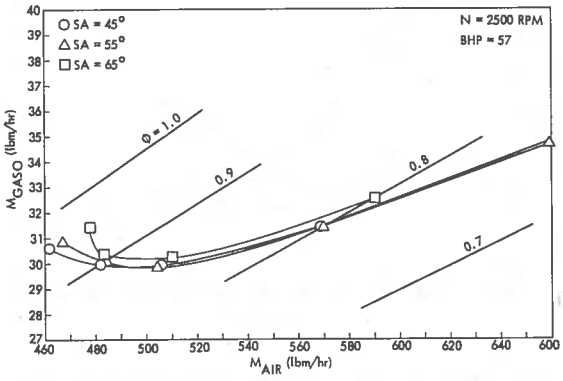

FIGURE C-14. FUEL CONSUMPTION CHARACTERISTIC (N=2500 RPM, BHP=57)

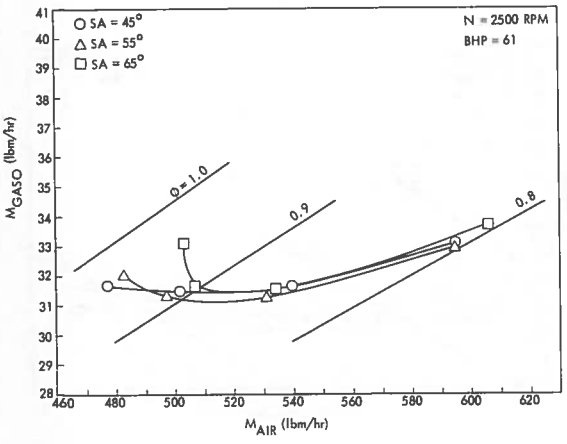

FIGURE C-15. FUEL CONSUMPTION CHARACTERISTIC (N=2500 RPM, BHP=61)

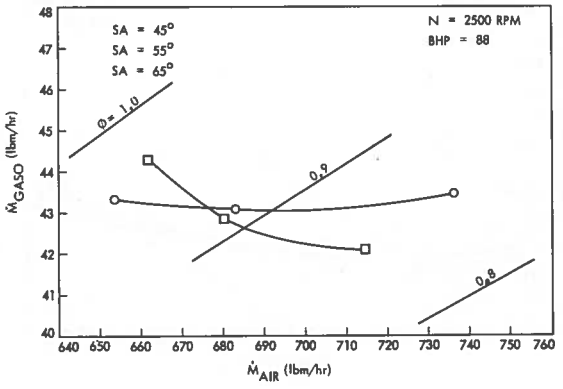

FIGURE C-16. FUEL CONSUMPTION CHARACTERISTIC (N=2500 RPM, BHP=88)

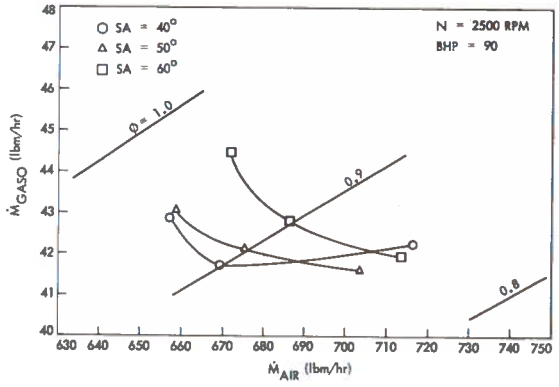

FIGURE C-17. FUEL CONSUMPTION CHARACTERISTIC (N=2500RPM, BHP=90)

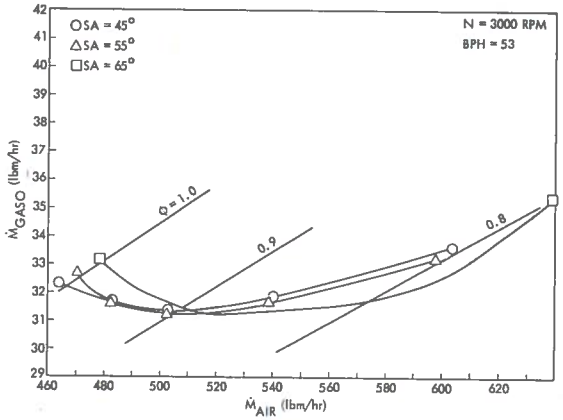

FIGURE C-18. FUEL CONSUMPTION CHARACTERISTIC (N=3000 RPM, BHP=53)

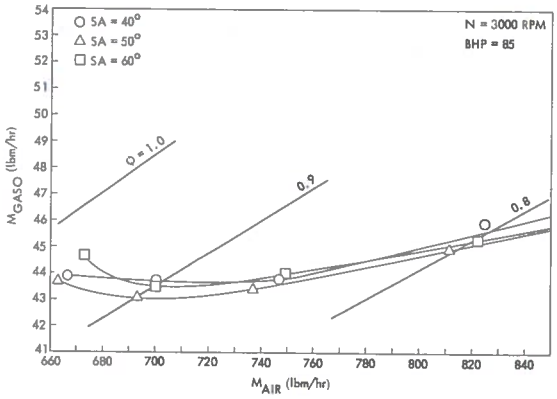

FIGURE C-19. FUEL CONSUMPTION CHARACTERISTIC (N=3000 RPM, BHP=85)

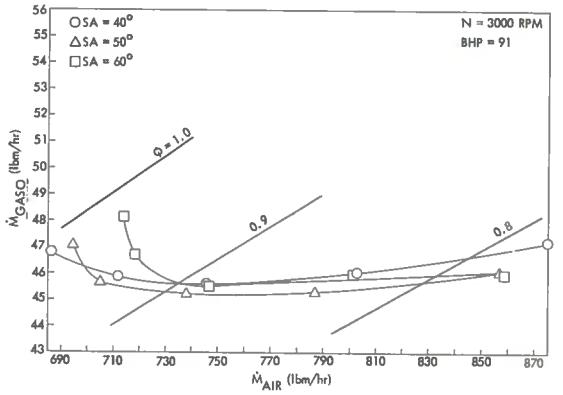

FIGURE C-20. FUEL CONSUMPTION CHARACTERISTIC (N=3000 RPM, BHP=91)

APPENDIX D

SENSITIVITY TEST DATA

FOR

LEAN BURN ENGINE CONFIGURATION No. 1

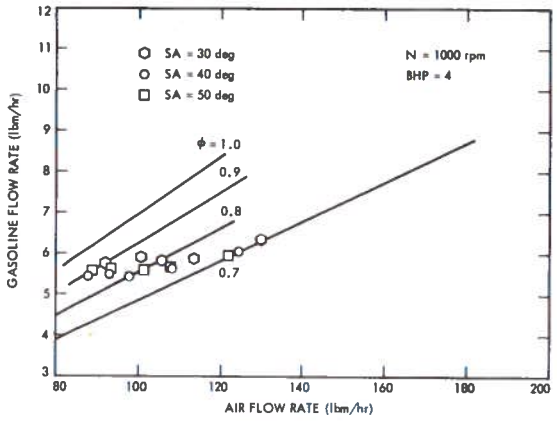

FIGURE D-1. FUEL CONSUMPTION CHARACTERISTIC FOR LBEC-2 (N=1000 RPM, BHP= 4)

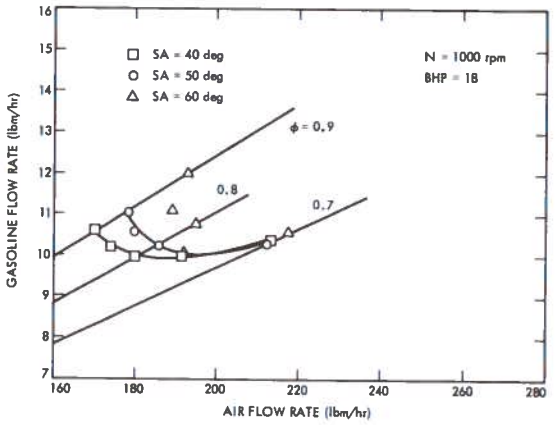

FIGURE D-2. FUEL CONSUMPTION CHARACTERISTIC FOR LBEC-2 (N=1000 RPM, BHP=18)

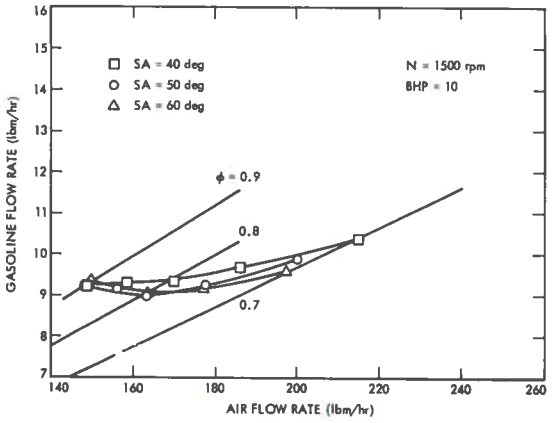

FIGURE D-3. FUEL CONSUMPTION CHARACTERISTIC FOR LBEC-2 (N=1500 RPM, BHP=10)

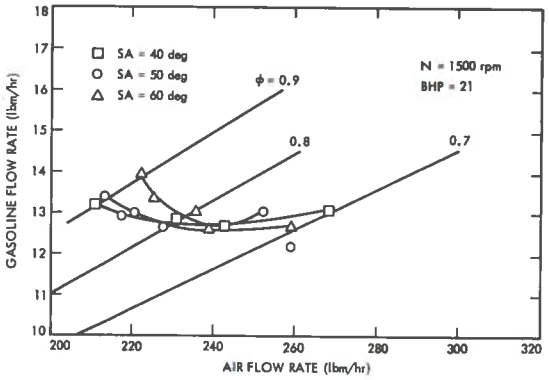

FIGURE D-4. FUEL CONSUMPTION CHARACTERISTIC FOR LBEC-2 (N=1500 RPM, BHP=21)

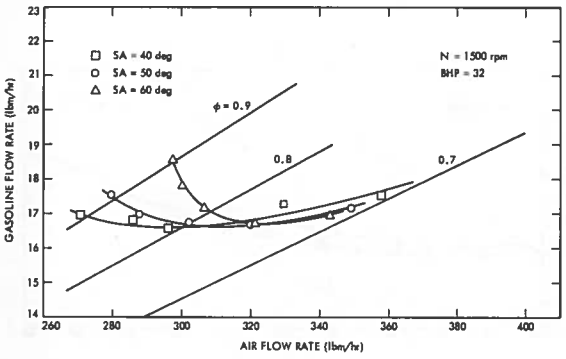

FIGURE D-5. FUEL CONSUMPTION CHARACTERISTIC FOR LBEC-2 (N=1500 RPM, BHP=32)

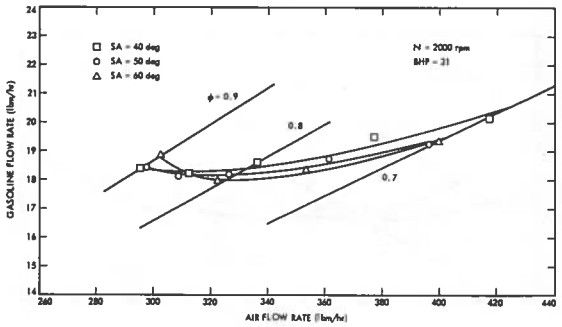

FIGURE D-6. FUEL CONSUMPTION CHARACTERISTIC FOR LBEC-2 (N=2000 RPM, BHP=31)

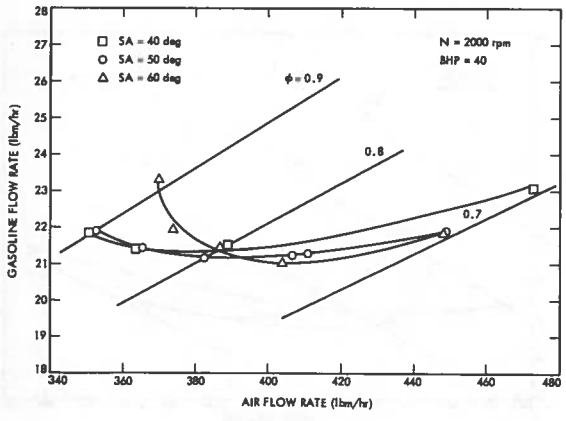

FIGURE D-7. FUEL CONSUMPTION CHARACTERISTIC FOR LBEC-2 (N=2000 RPM, BHP=40)

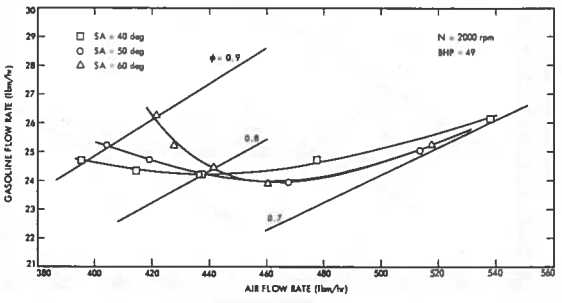

FIGURE D-8. FUEL CONSUMPTION CHARACTERISTIC FOR LBEC-2 (N=2000 RPM, BHP=49)

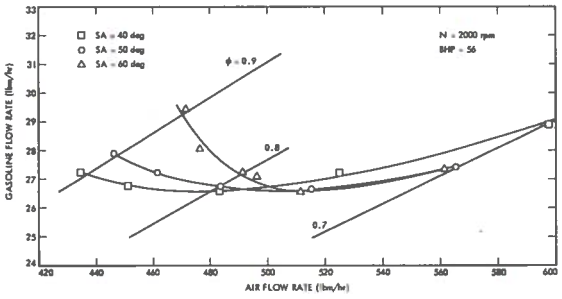

FIGURE D-9. FUEL CONSUMPTION CHARACTERISTIC FOR LBEC-2 (N=2000 RPM, BHP=56)

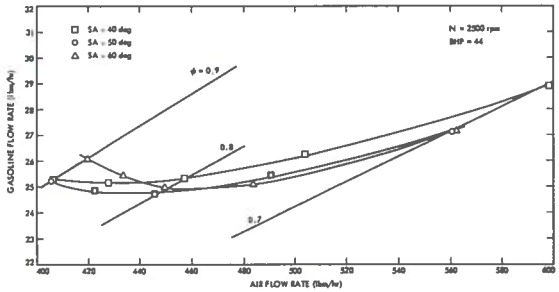

FIGURE D-10. FUEL CONSUMPTION CHARACTERISTIC FOR LBEC-2 (N=2500 RPM, BHP=44)

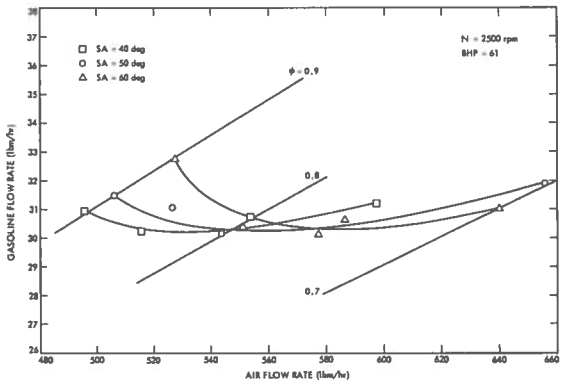

FIGURE D-11. FUEL CONSUMPTION CHARACTERISTIC FOR LBEC-2 (N=2500 RPM, BHP=61)

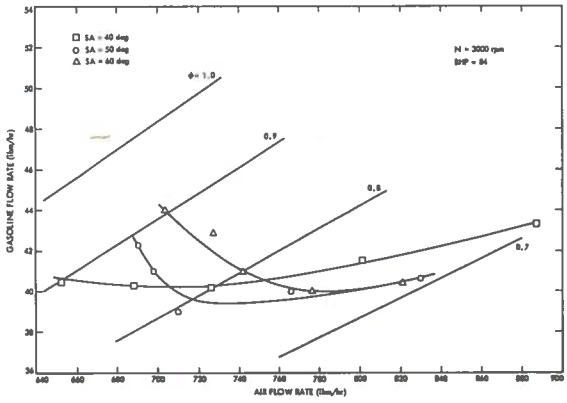

FIGURE D-12. FUEL CONSUMPTION CHARACTERISTIC FOR LBEC-2 (N=3000 RPM, BHP=84)

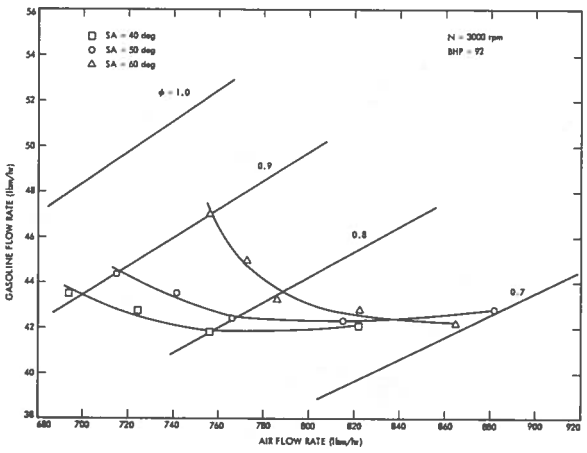

FIGURE D-13. FUEL CONSUMPTION CHARACTERISTIC FOR LBEC-2 (N=3000 RPM, BHP=92)

APPENDIX E

MAPPING TEST DATA FOR
LEAN BURN ENGINE CONFIGURATION NO. 2

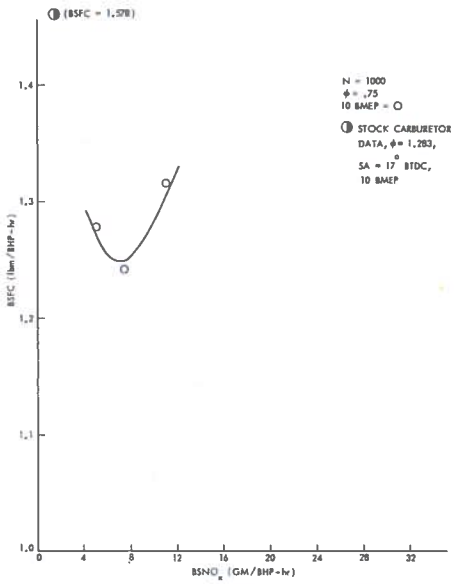

FIGURE E-1. LOAD EFFECTS ON BSFC VERSUS BSNO$_x$ CHARACTERISTIC (N = 1000)

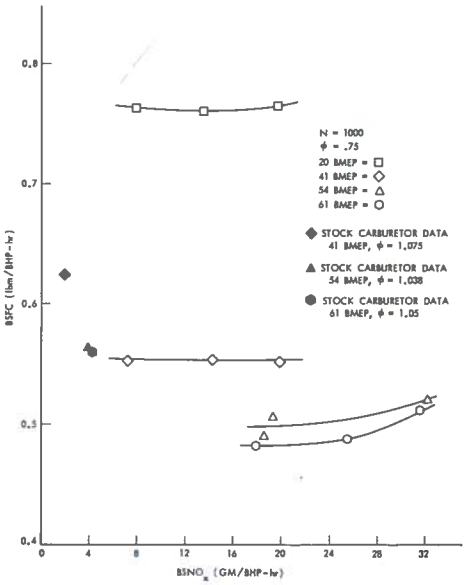

FIGURE E-2. LOAD EFFECTS ON BSFC VERSUS BSNO$_x$ CHARACTERISTIC (N = 1000)

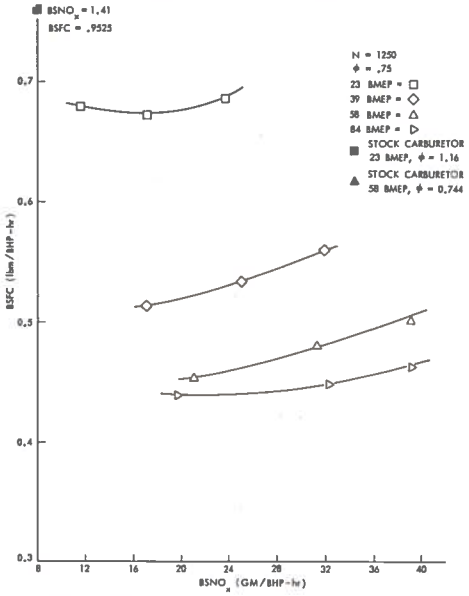

FIGURE E-3. LOAD EFFECTS ON BSFC VERSUS BSNO$_x$ CHARACTERISTIC (N = 1250)

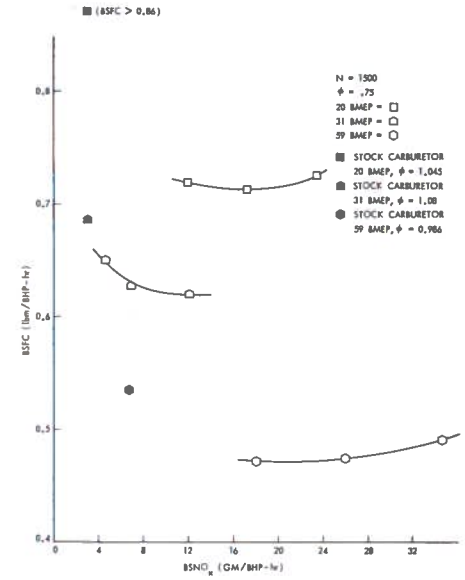

FIGURE E-4. LOAD EFFECTS ON BSFC VERSUS BSNO$_x$ CHARACTERISTIC (N = 1500)

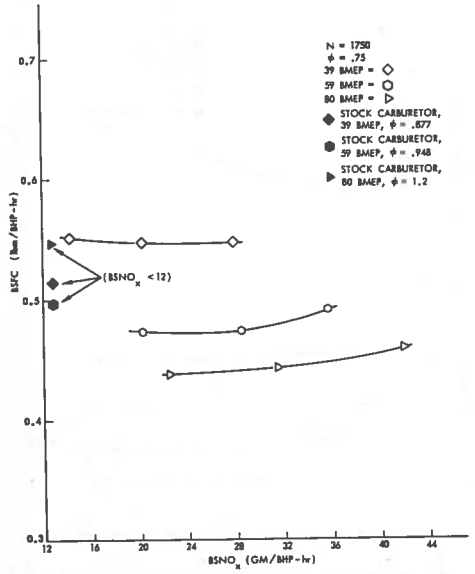

FIGURE E-5. LOAD EFFECTS ON BSFC VERSUS BSNO$_x$ CHARACTERISTIC (N = 1750)

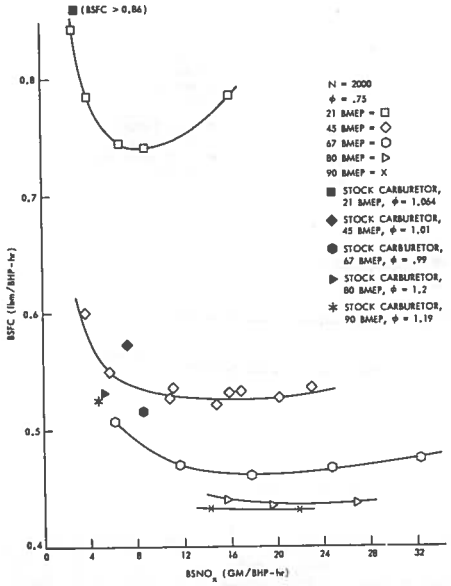

FIGURE E-6. LOAD EFFECTS ON BSFC VERSUS BSNO$_x$ CHARACTERISTIC (N = 2000)

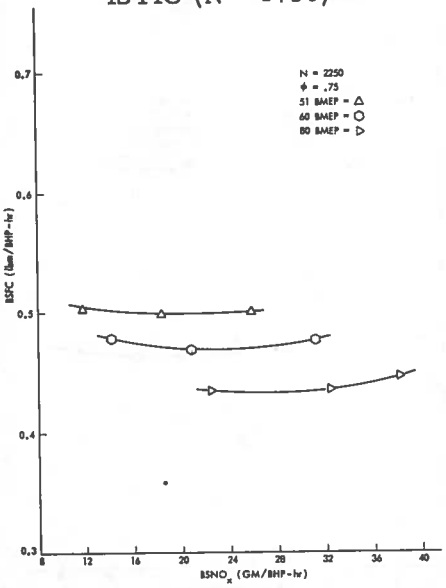

FIGURE E-7. LOAD EFFECTS ON BSFC VERSUS BSNO$_x$ CHARACTERISTIC (N = 2250)

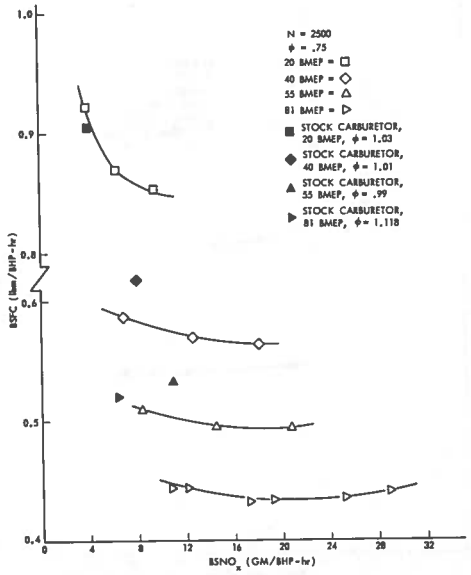

FIGURE E-8. LOAD EFFECTS ON BSFC VERSUS BSNO$_x$ CHARACTERISTIC (N = 2500)

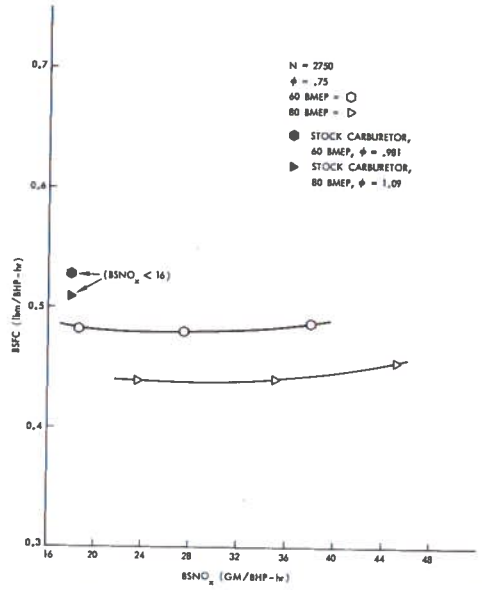

FIGURE E-9. LOAD EFFECTS ON BSFC VERSUS BSNO$_x$ CHARACTERISTIC (N = 2750)

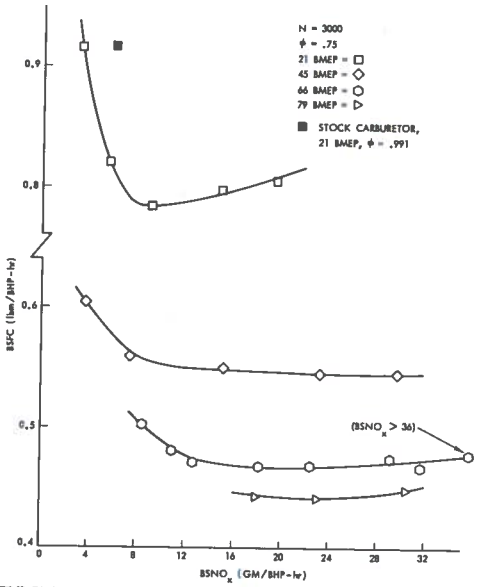

FIGURE E-10. LOAD EFFECTS ON BSFC VERSUS BSNO$_x$ CHARACTERISTIC (N = 3000)

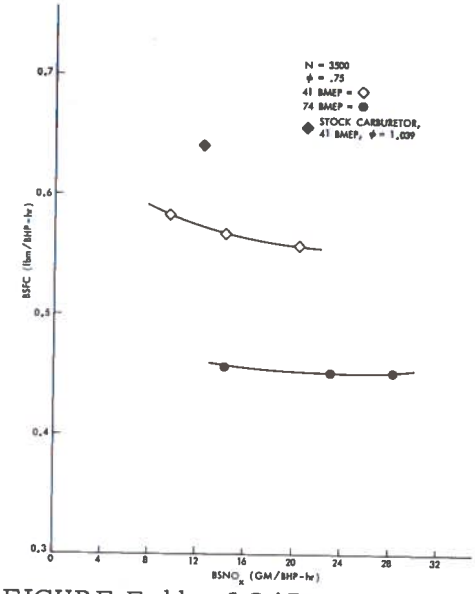

FIGURE E-11. LOAD EFFECTS ON BSFC VERSUS BSNO$_x$ CHARACTERISTIC (N = 3500)

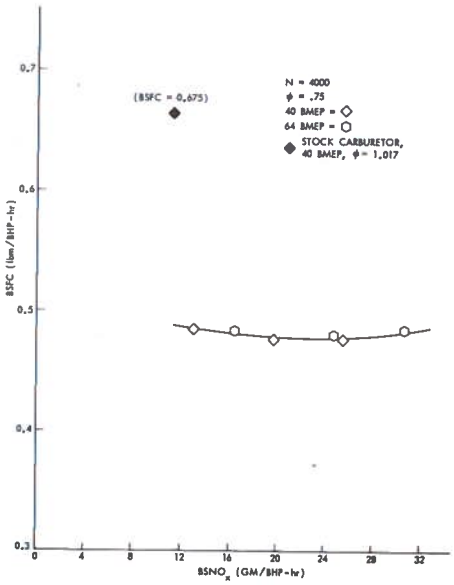

FIGURE E-12. LOAD EFFECTS ON BSFC VERSUS BSNO$_x$ CHARACTERISTIC (N = 4000)

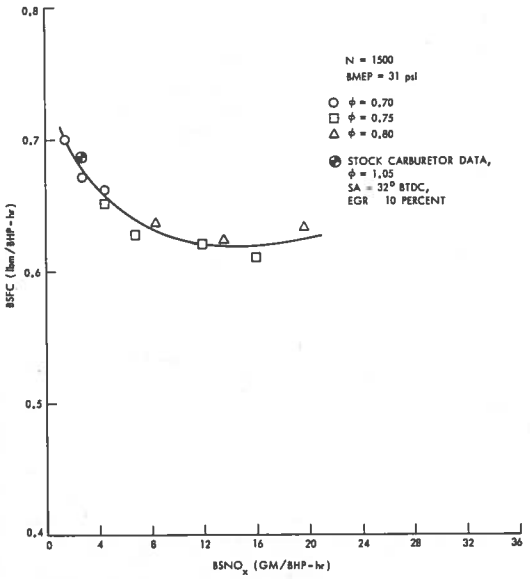

FIGURE E-13. BSFC VERSUS BSNO$_x$ CHARACTERISTIC (N = 1500, BMEP = 31 psi)

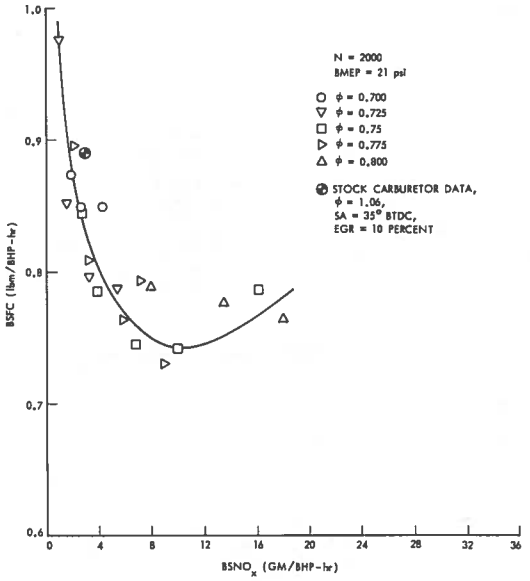

FIGURE E-14. BSFC VERSUS BSNO$_x$ CHARACTERISTIC (N = 2000, BNEO = 21 psi)

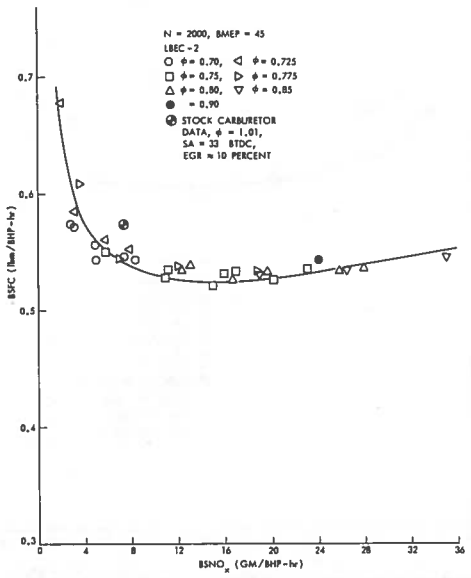

FIGURE E-15. BSFC VERSUS BSNO$_x$ CHARACTERISTIC (N = 2000, BMEP = 45 psi)

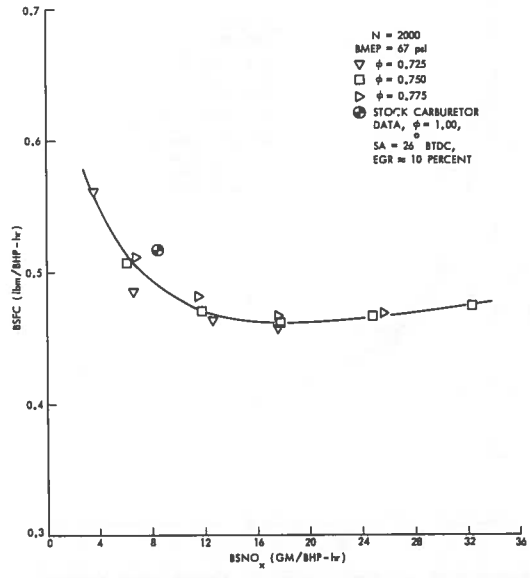

FIGURE E-16. BSFC VERSUS BSNO$_x$ CHARACTERISTIC (N = 2000, BMEP = 67 psi)

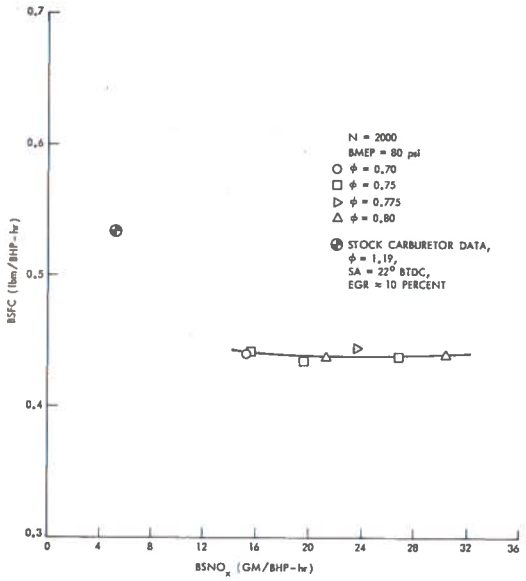

FIGURE E-17. BSFC VERSUS BSNO$_x$ CHARACTERISTIC (N = 2000, BMEP = 80 psi)

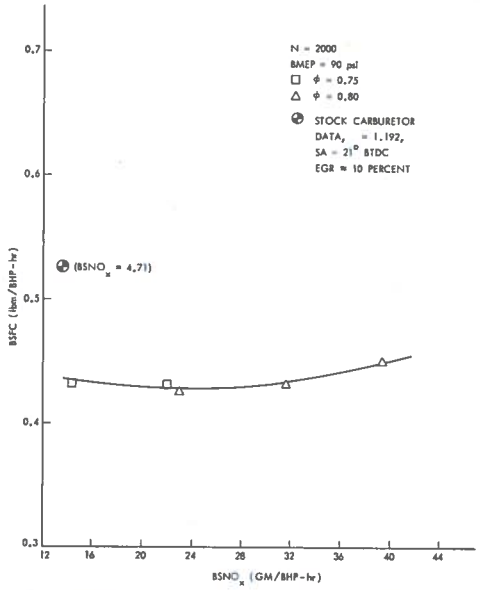

FIGURE E-18. BSFC VERSUS BSNO$_x$ CHARACTERISTIC (N = 2000, BMEP = 90 psi)

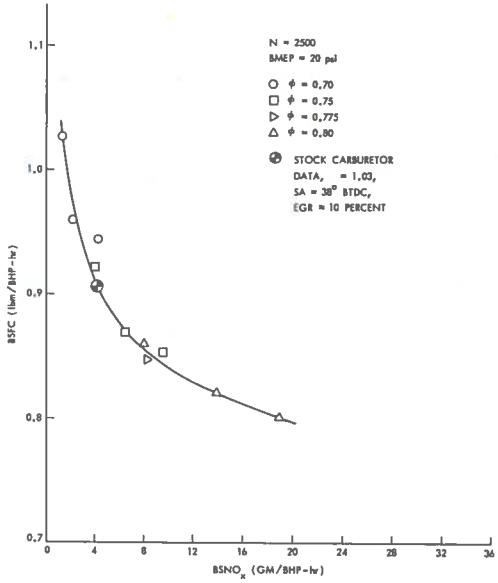

FIGURE E-19. BSFC VERSUS BSNO$_x$ CHARACTERISTIC (N = 2500, BMEP = 20 psi)

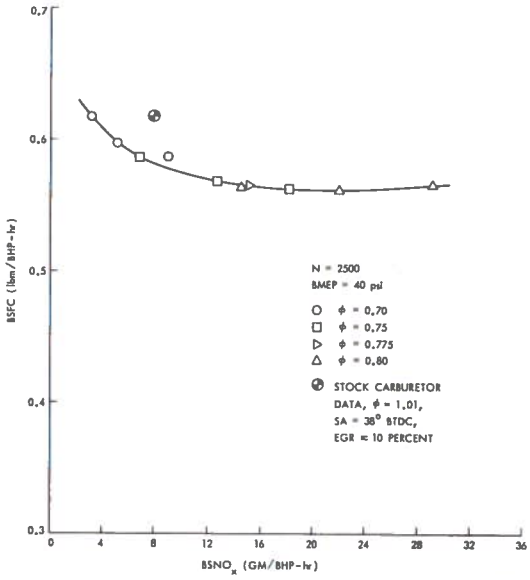

FIGURE E-20. BSFC VERSUS BSNO$_x$ CHARACTERISTIC (N = 2500, BMEP = 40 psi)

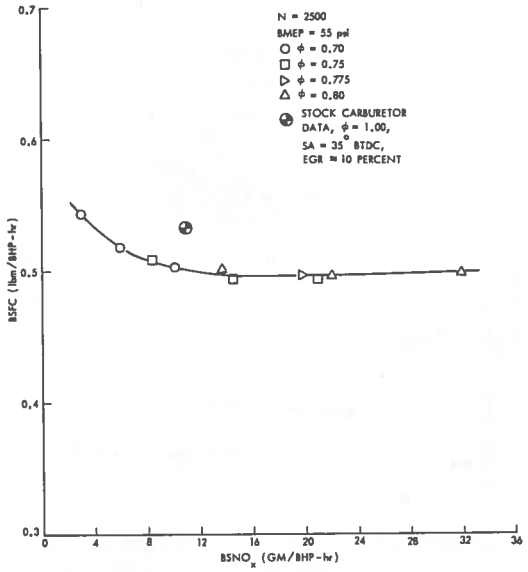

FIGURE E-21. BSFC VERSUS BSNO$_x$ CHARACTERISTIC (N = 2500, BMEP = 55 psi)

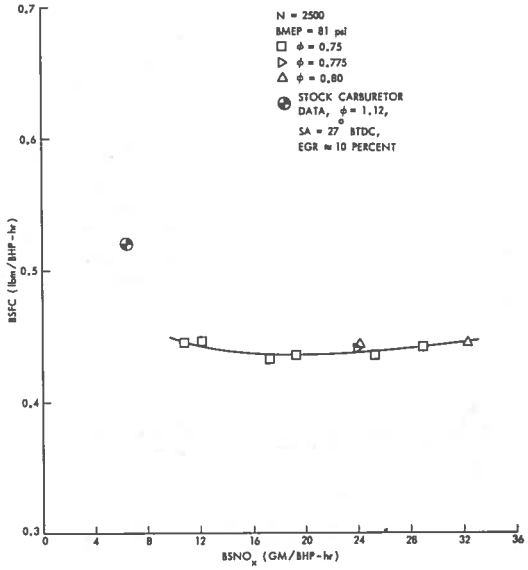

FIGURE E-22. BSFC VERSUS BSNO$_x$ CHARACTERISTIC (N = 2500, BMEP = 81 psi)

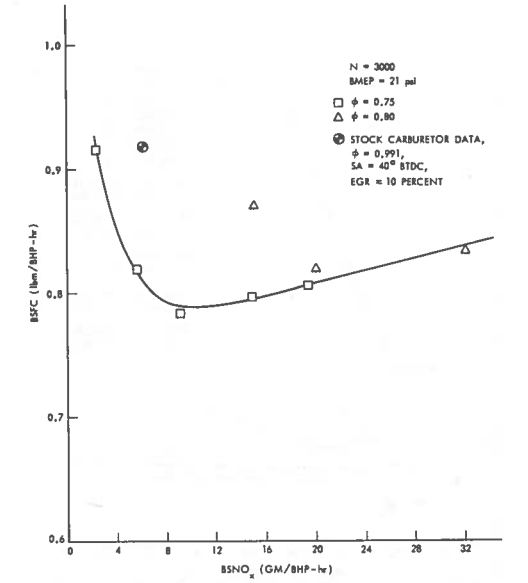

FIGURE E-23. BSFC VERSUS BSNO$_x$ CHARACTERISTIC (N = 3000, BMEP = 21 psi)

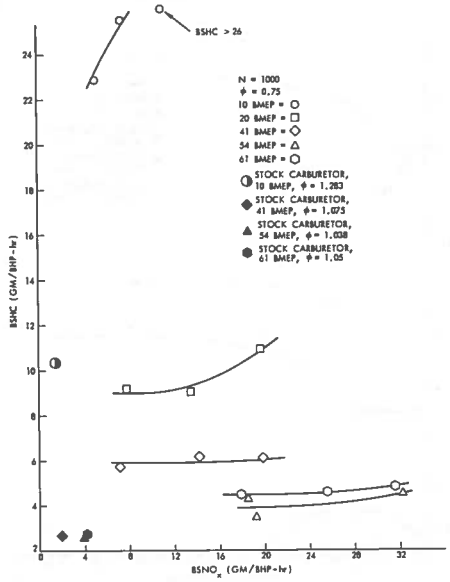

FIGURE E-24. LOAD EFFECTS ON BSHC VERSUS BSNO$_x$ CHARACTERISTIC (N = 1000)

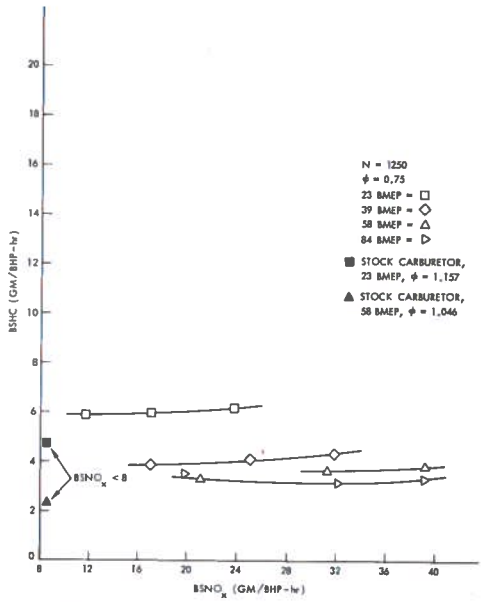

FIGURE E-25. LOAD EFFECTS ON BSHC VERSUS BSNO$_x$ CHARACTERISTIC (N = 1250)

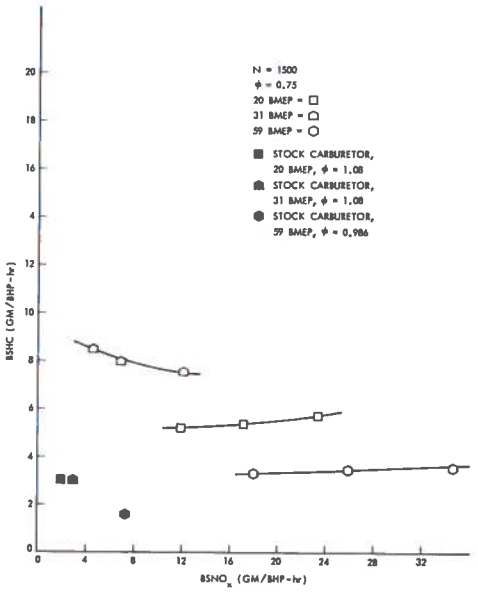

FIGURE E-26. LOAD EFFECTS ON BSHC VERSUS BSNO$_x$ CHARACTERISTIC (N = 1500)

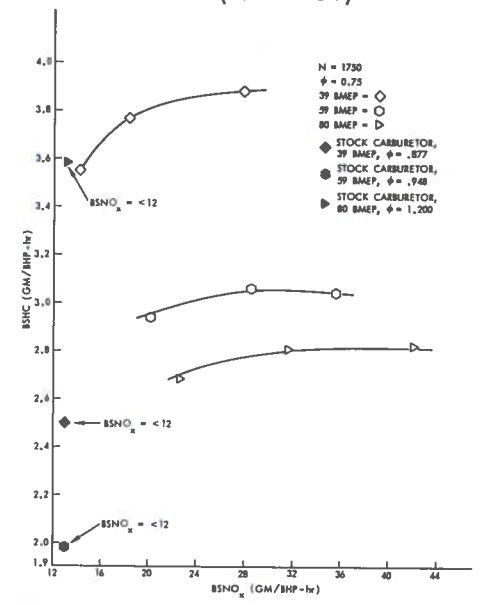

FIGURE E-27. LOAD EFFECTS ON BSHC VERSUS BSNO$_x$ CHARACTERISTIC (N = 1750)

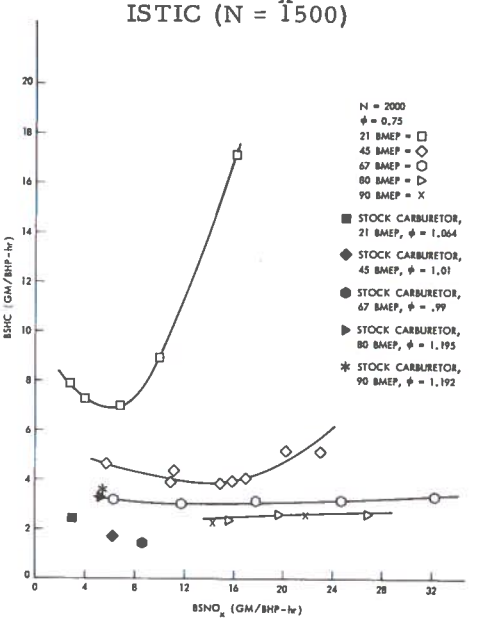

FIGURE E-28. LOAD EFFECTS ON BSHC VERSUS BSNO$_x$ CHARACTERISTIC (N = 2000)

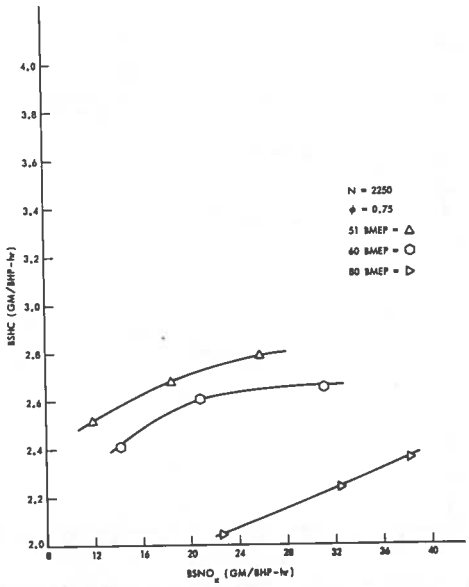

FIGURE E-29. LOAD EFFECTS ON BSHC VERSUS BSNO$_x$ CHARACTERISTIC (N = 2250)

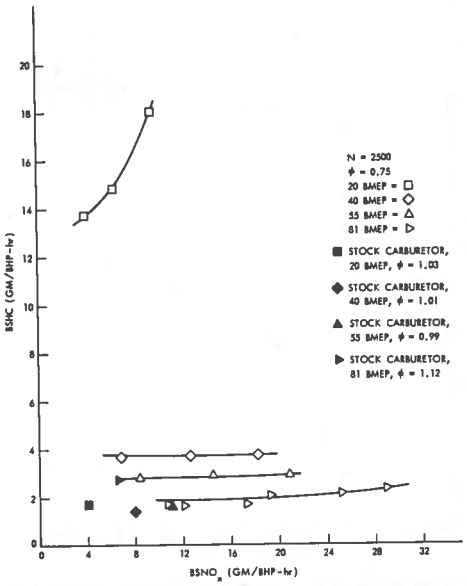

FIGURE E-30. LOAD EFFECTS ON BSHC VERSUS BSNO$_x$ CHARACTERISTIC (N = 2500)

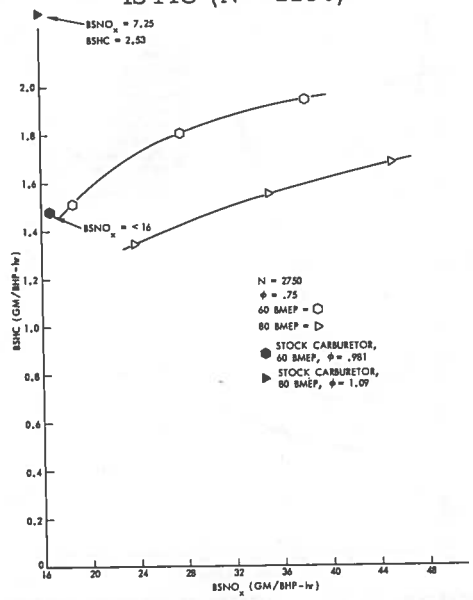

FIGURE E-31. LOAD EFFECTS ON BSHC VERSUS BSNO$_x$ CHARACTERISTIC (N = 2750)

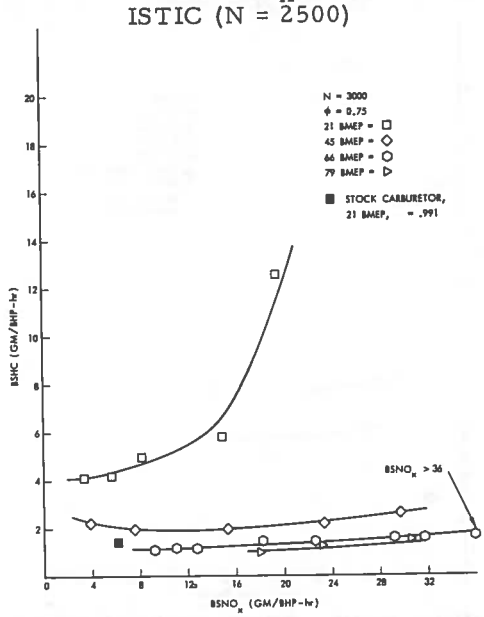

FIGURE E-32. LOAD EFFECTS ON BSHC VERSUS BSNO$_x$ CHARACTERISTIC (N = 3000)

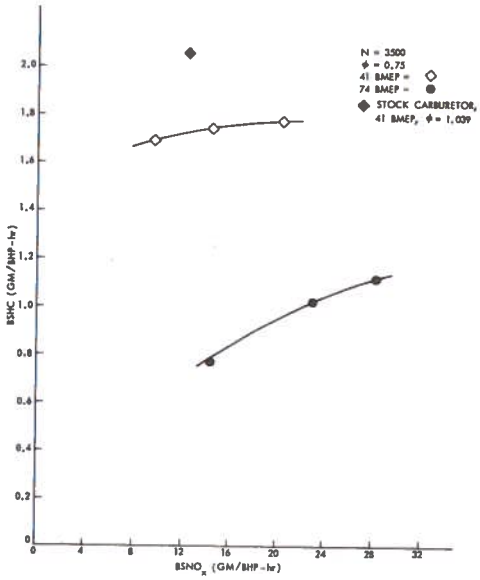

FIGURE E-33. LOAD EFFECTS ON BSHC VERSUS BSNO$_x$ CHARACTERISTIC (N = 3500)

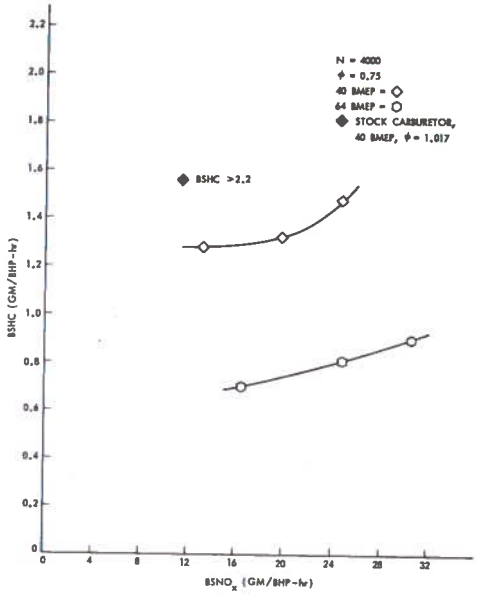

FIGURE E-34. LOAD EFFECTS ON BSHC VERSUS BSNO$_x$ CHARACTERISTIC (N = 4000)

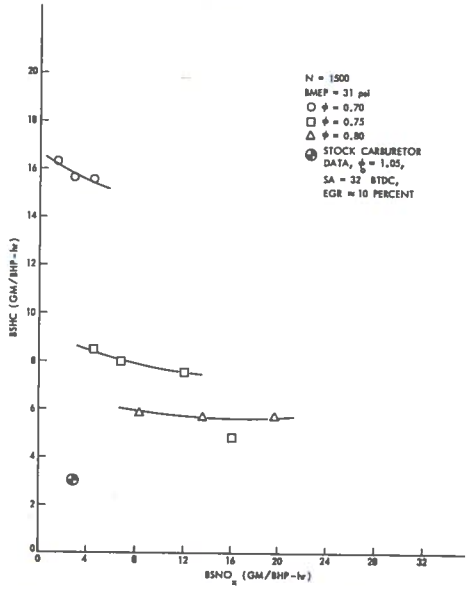

FIGURE E-35. BSHC VERSUS BSNO$_x$ CHARACTERISTIC (N = 1500, BMEP = 31 psi)

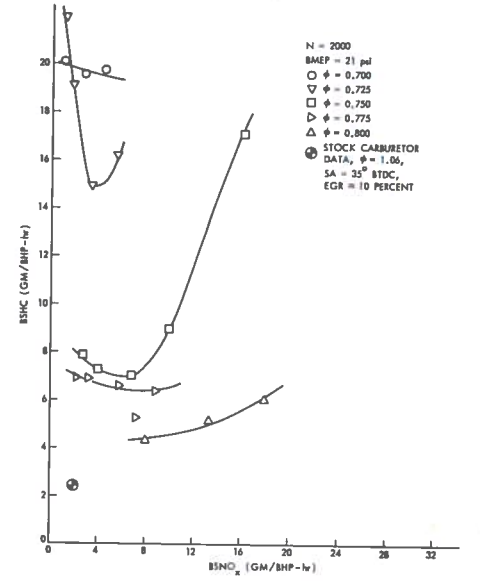

FIGURE E-36. BSHC VERSUS BSNO$_x$ CHARACTERISTIC (N = 2000, BMEP = 21 psi)

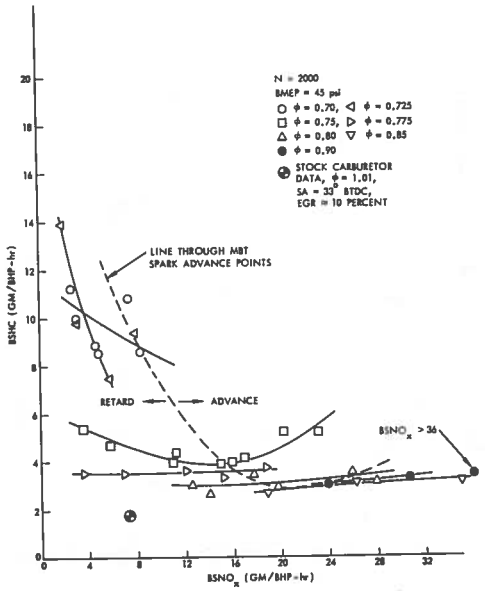

FIGURE E-37. BSHC VERSUS BSNO$_x$ CHARACTERISTIC (N = 2000, BMEP = 45 psi)

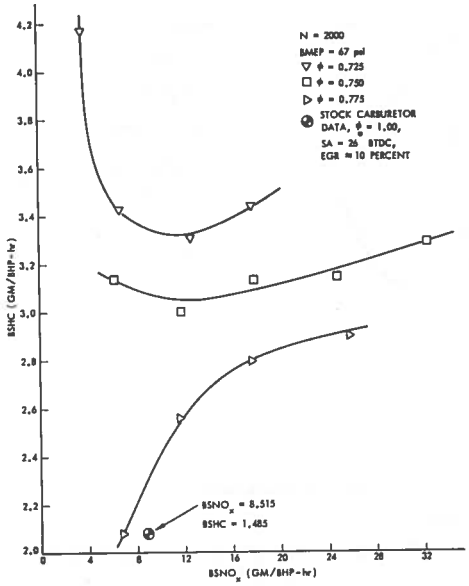

FIGURE E-38. BSHC VERSUS BSNO$_x$ CHARACTERISTIC (N = 2000, BMEP = 67 psi)

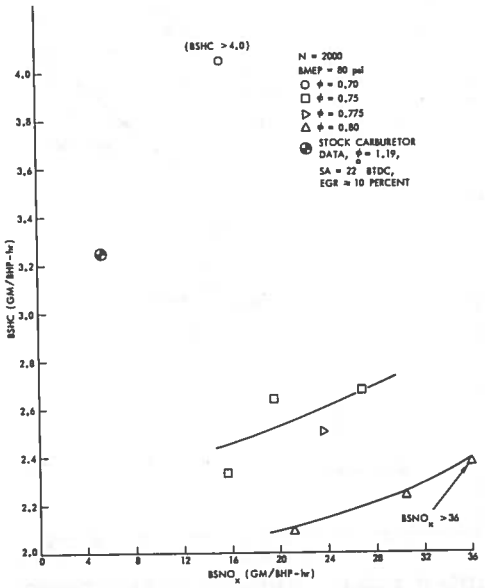

FIGURE E-39. BSHC VERSUS BSNO$_x$ CHARACTERISTIC (N = 2000, BMEP = 80 psi)

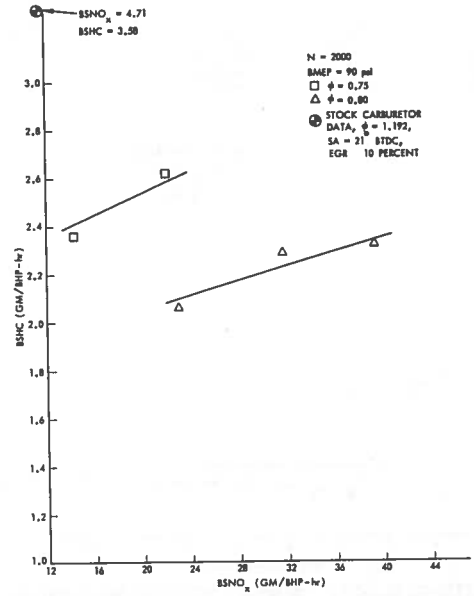

FIGURE E-40. BSHC VERSUS BSNO$_x$ CHARACTERISTIC (N = 2000, BMEP = 90 psi)

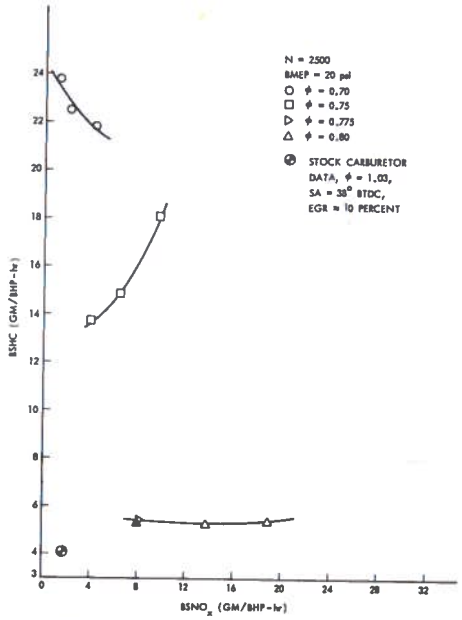

FIGURE E-41. BSHC VERSUS BSNO$_x$ CHARACTERISTIC (N = 2500, BMEP = 20 psi)

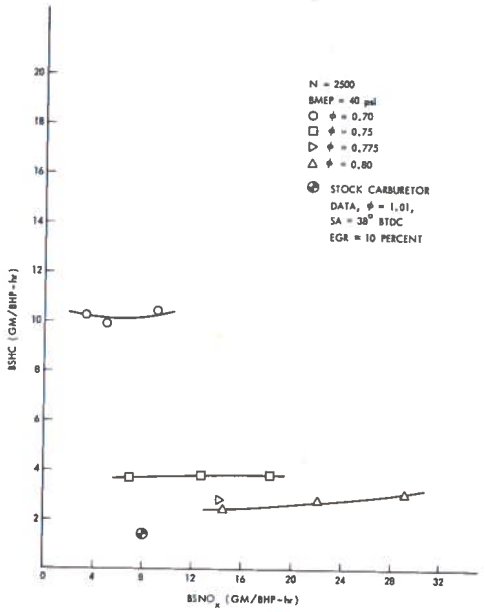

FIGURE E-42. BSHC VERSUS BSNO$_x$ CHARACTERISTIC (N = 2500, BMEP = 40 psi)

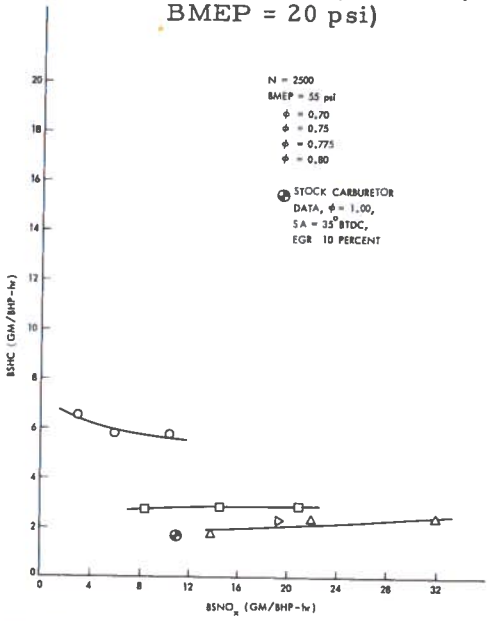

FIGURE E-43. BSHC VERSUS BSNO$_x$ CHARACTERISTIC (N = 2500, BMEP = 55 psi)

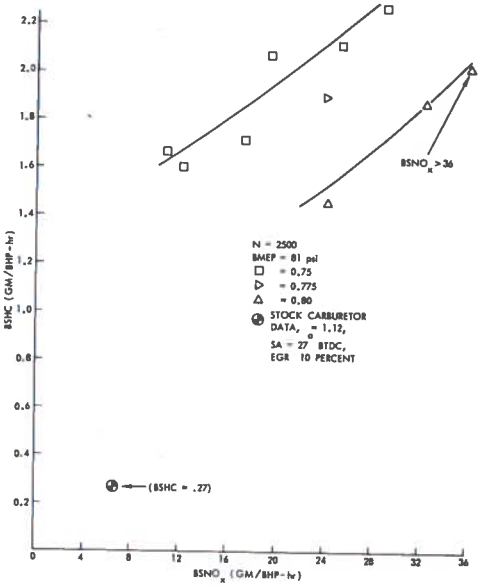

FIGURE E-44. BSHC VERSUS BSNO$_x$ CHARACTERISTIC (N = 2500, BMEP = 81 psi)

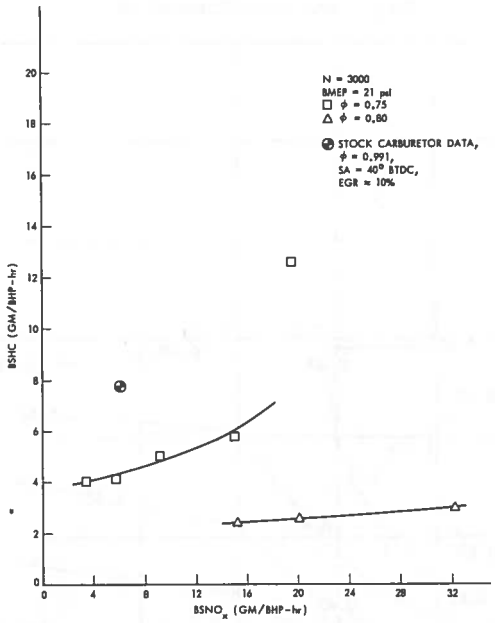

FIGURE E-45. BSHC VERSUS BSNO$_x$ CHARACTERISTIC (N = 3000, BMEP = 21 psi)

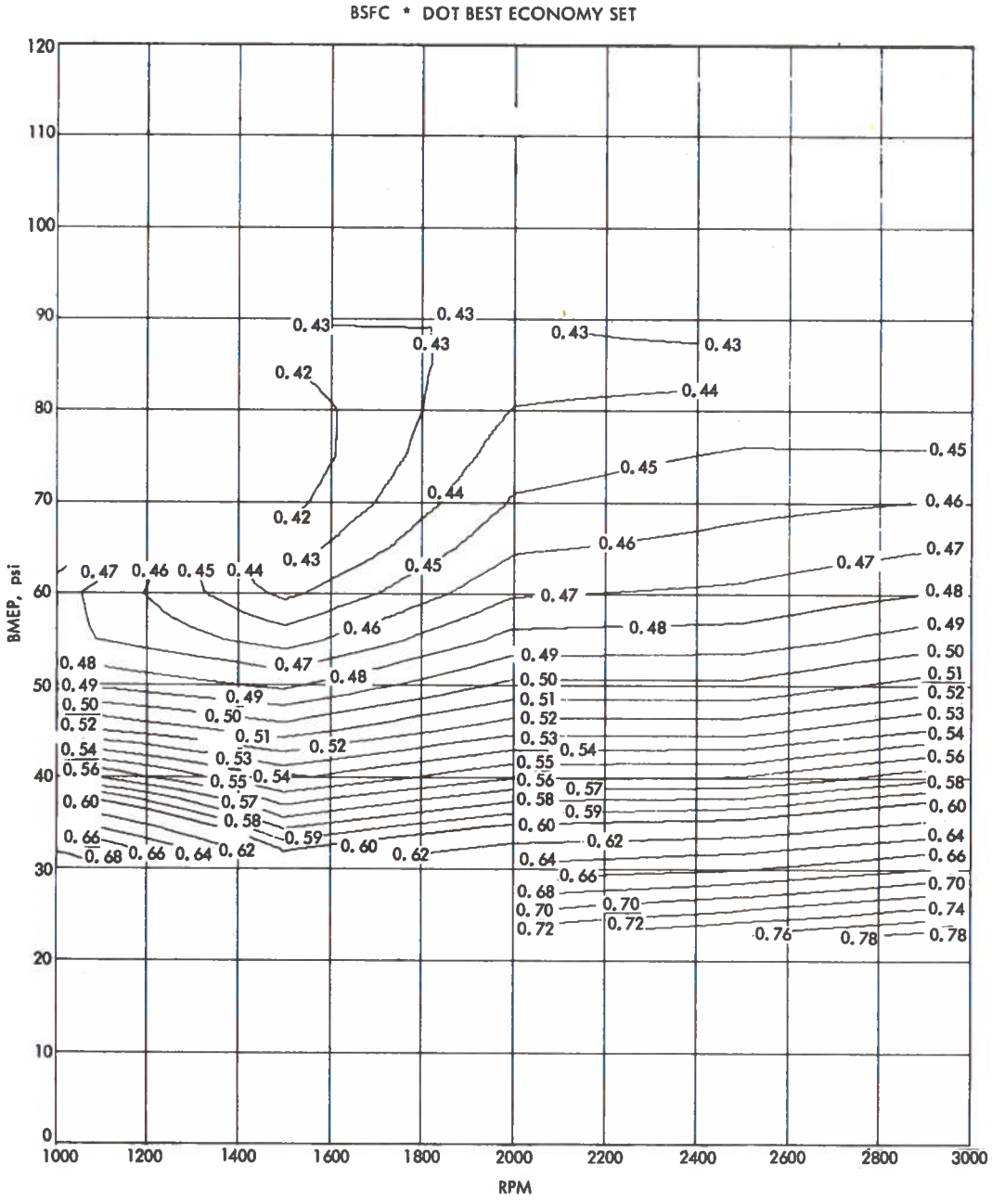

FIGURE E-46. BSFC CONTOUR MAP FOR LBEC-2 ENGINE (BEST ECONOMY SET)

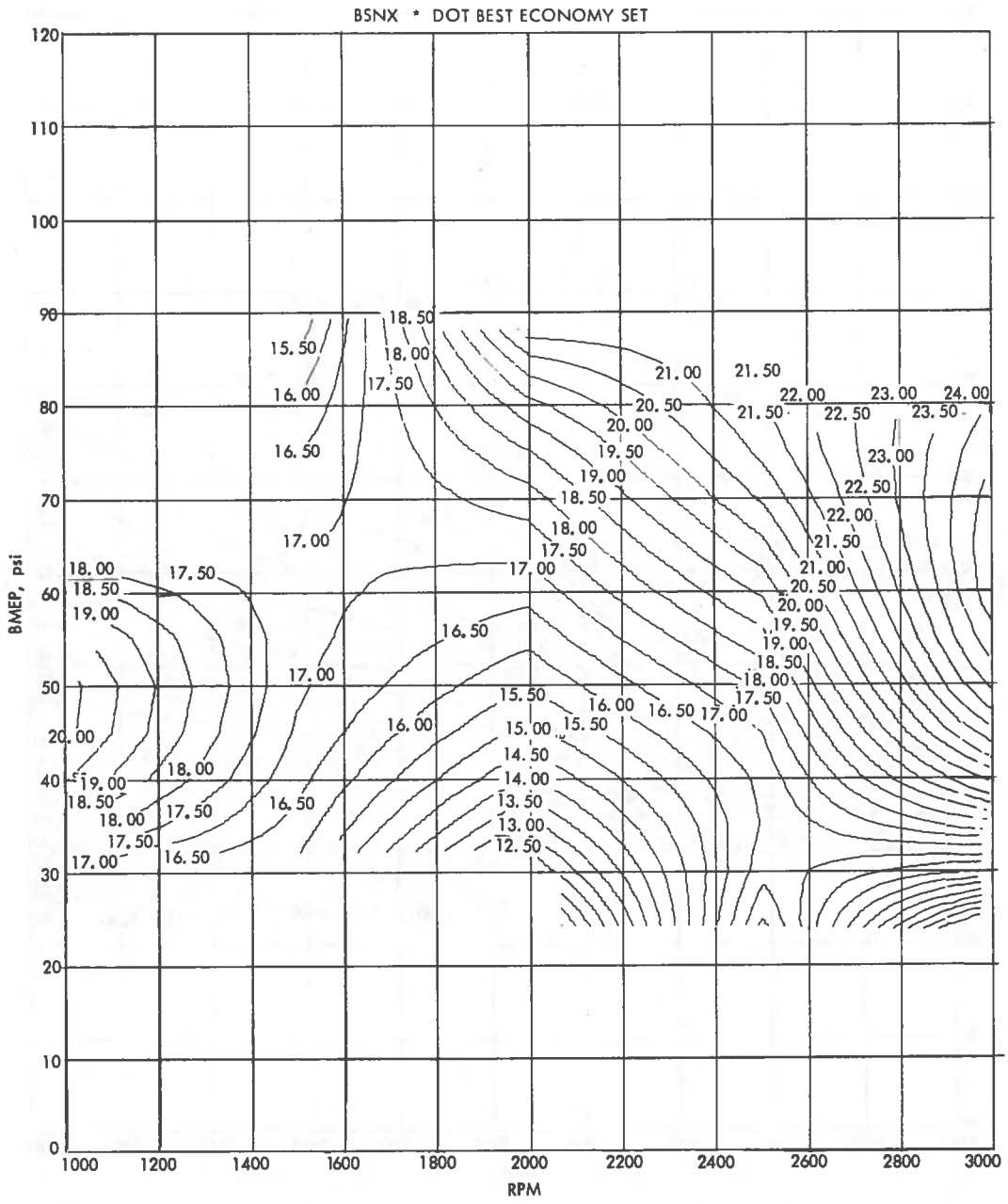

FIGURE E-47. $BSNO_x$ CONTOUR MAP FOR LBEC-2 ENGINE (BEST ECONOMY SET)

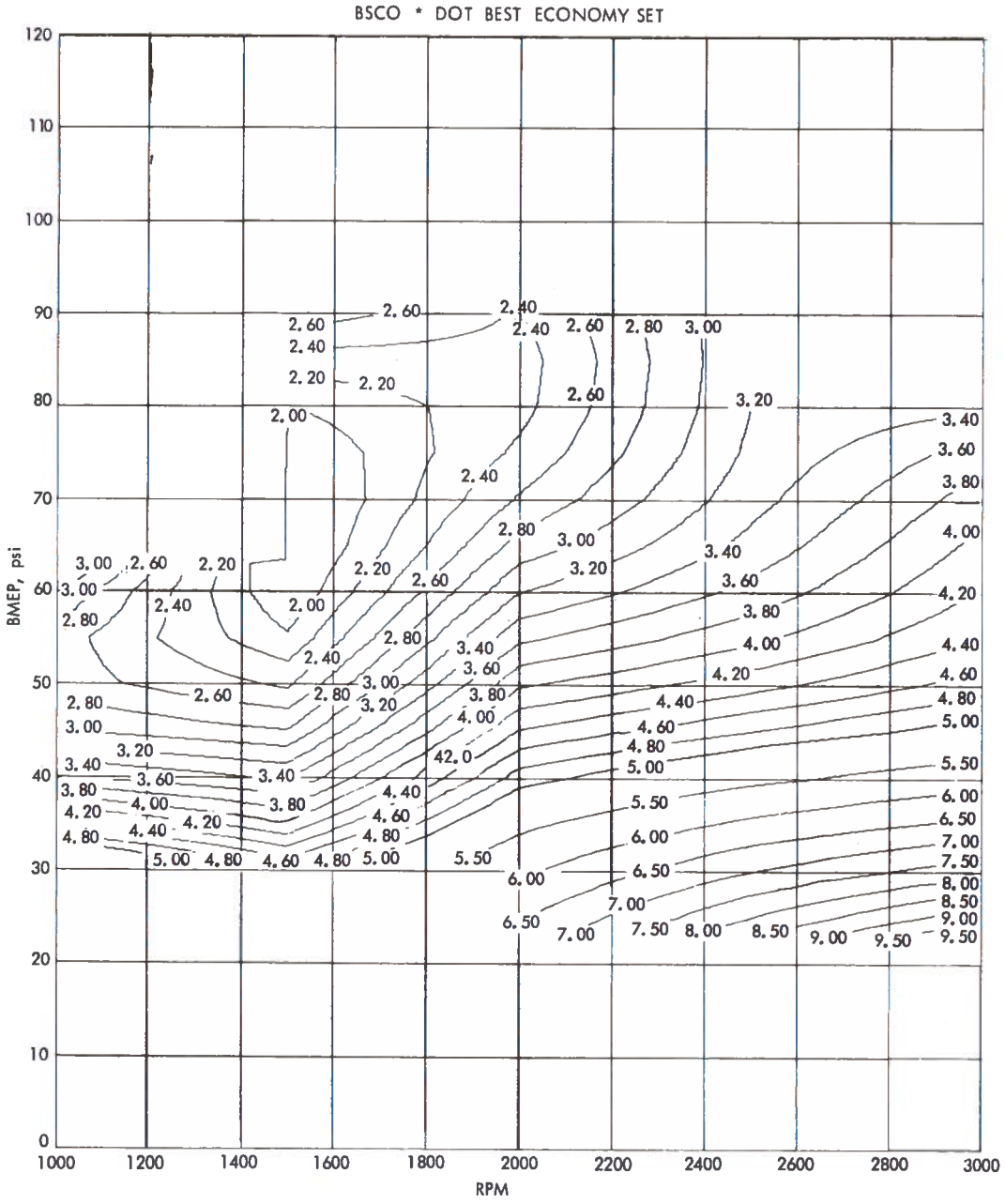

FIGURE E-48. BSCO CONTOUR MAP FOR LBEC-2 ENGINE (BEST ECONOMY SET)

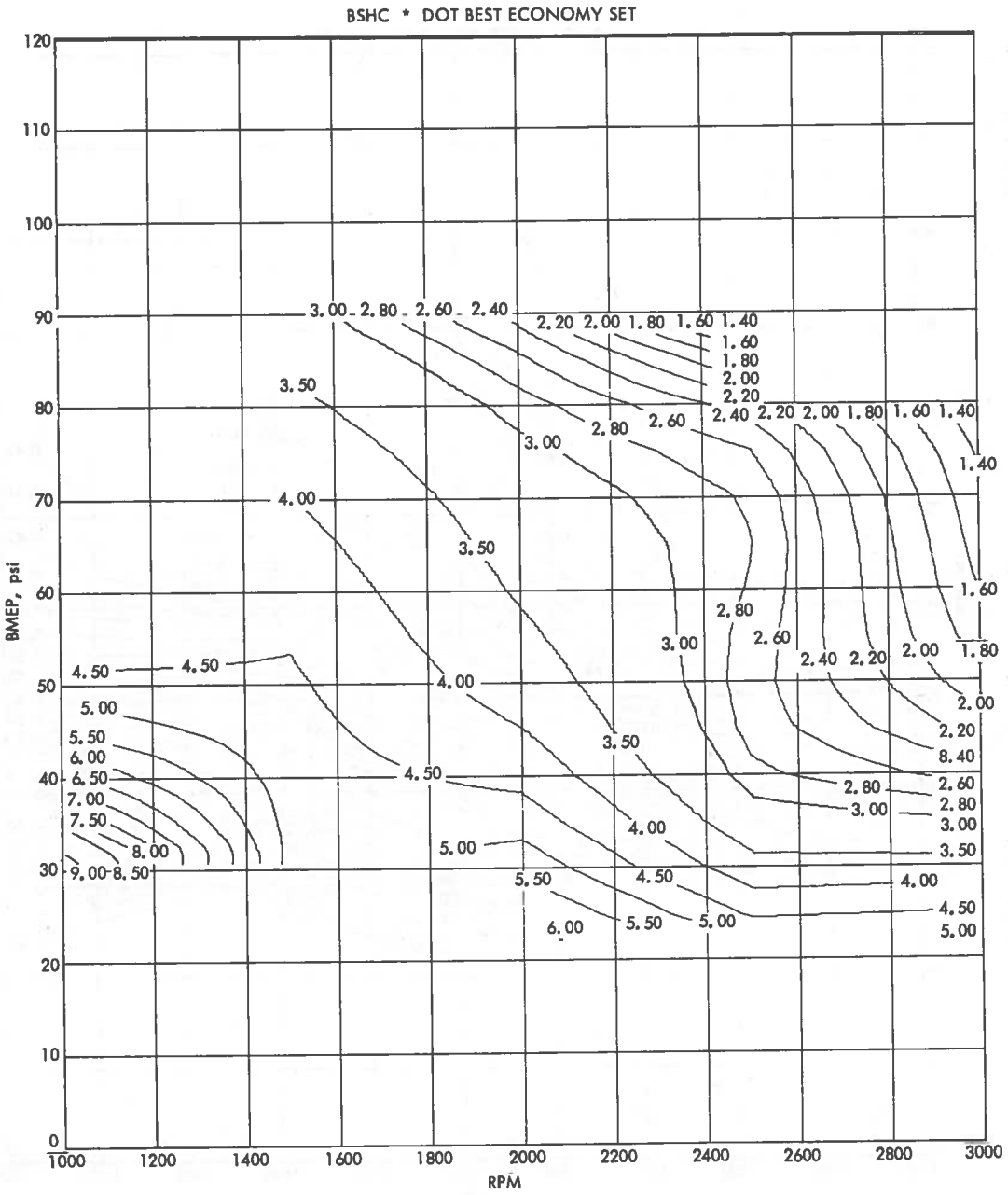

FIGURE E-49. BSHC CONTOUR MAP FOR LBEC-2 ENGINE (BEST ECONOMY SET)

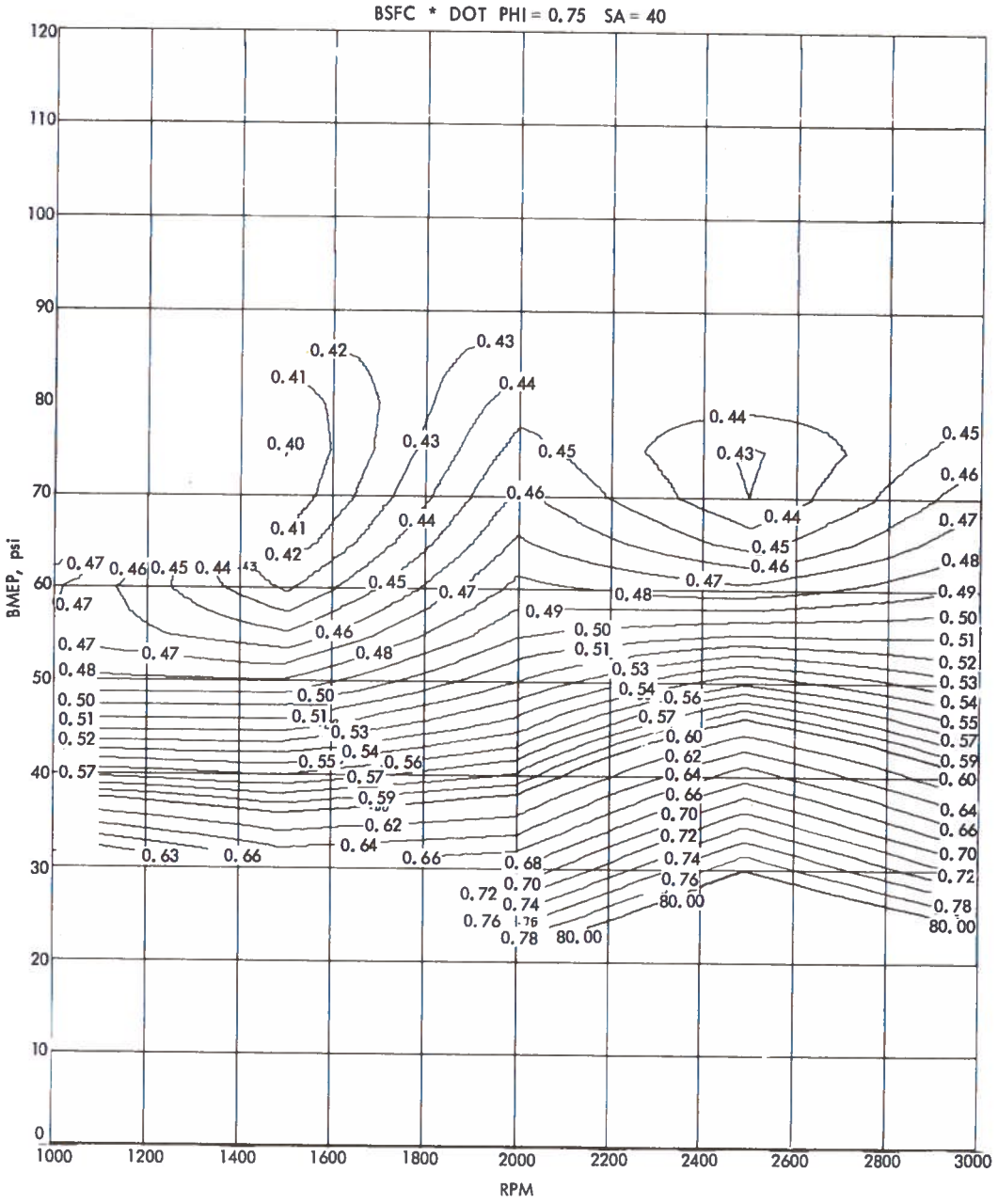

FIGURE E-50. BSFC CONTOUR MAP FOR LBEC-2 ENGINE
(Φ = .75, SA = 40)

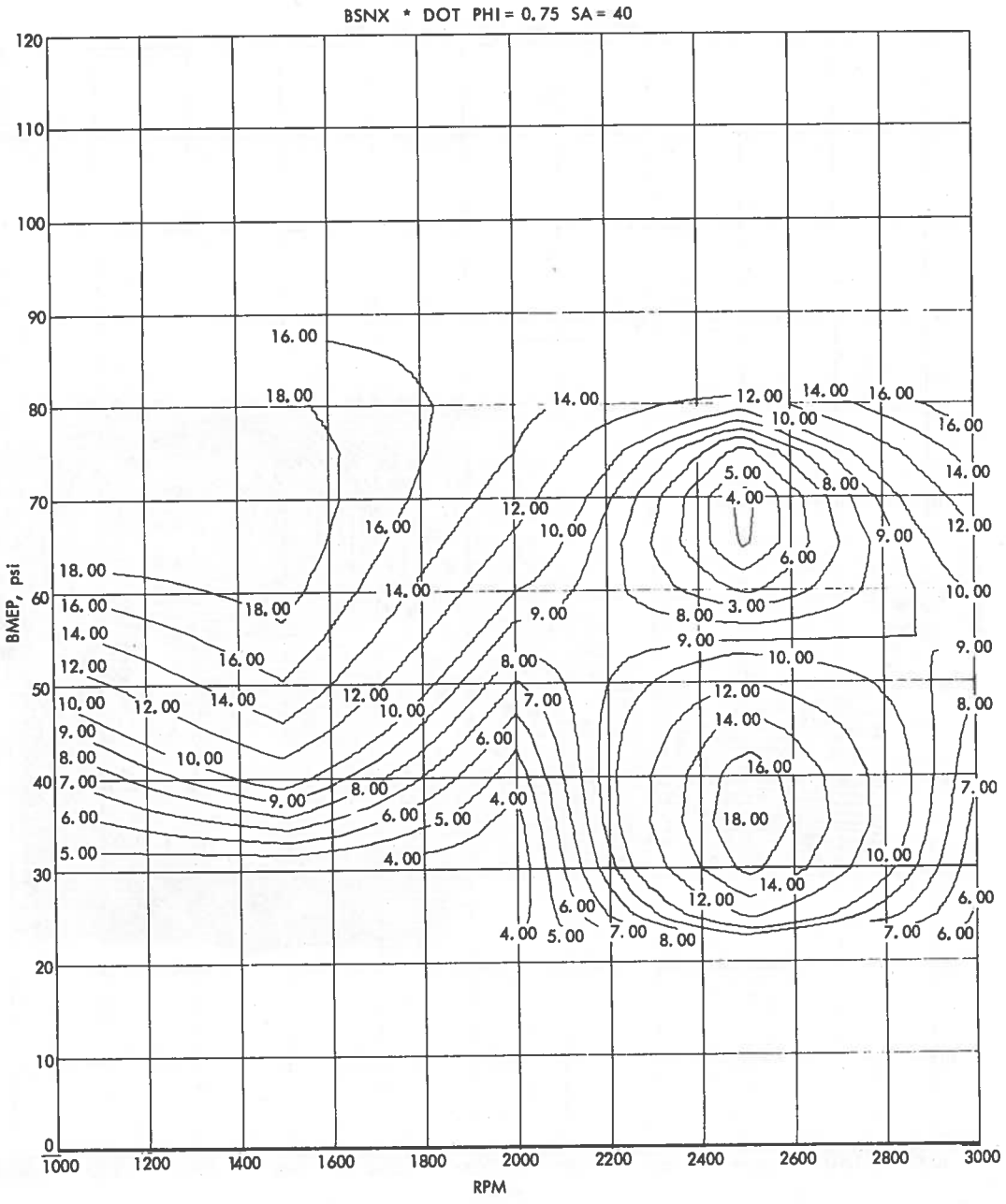

FIGURE E-51. $BSNO_x$ CONTOUR MAP FOR LBEC-2 ENGINE
(Φ = .75, SA = 40)

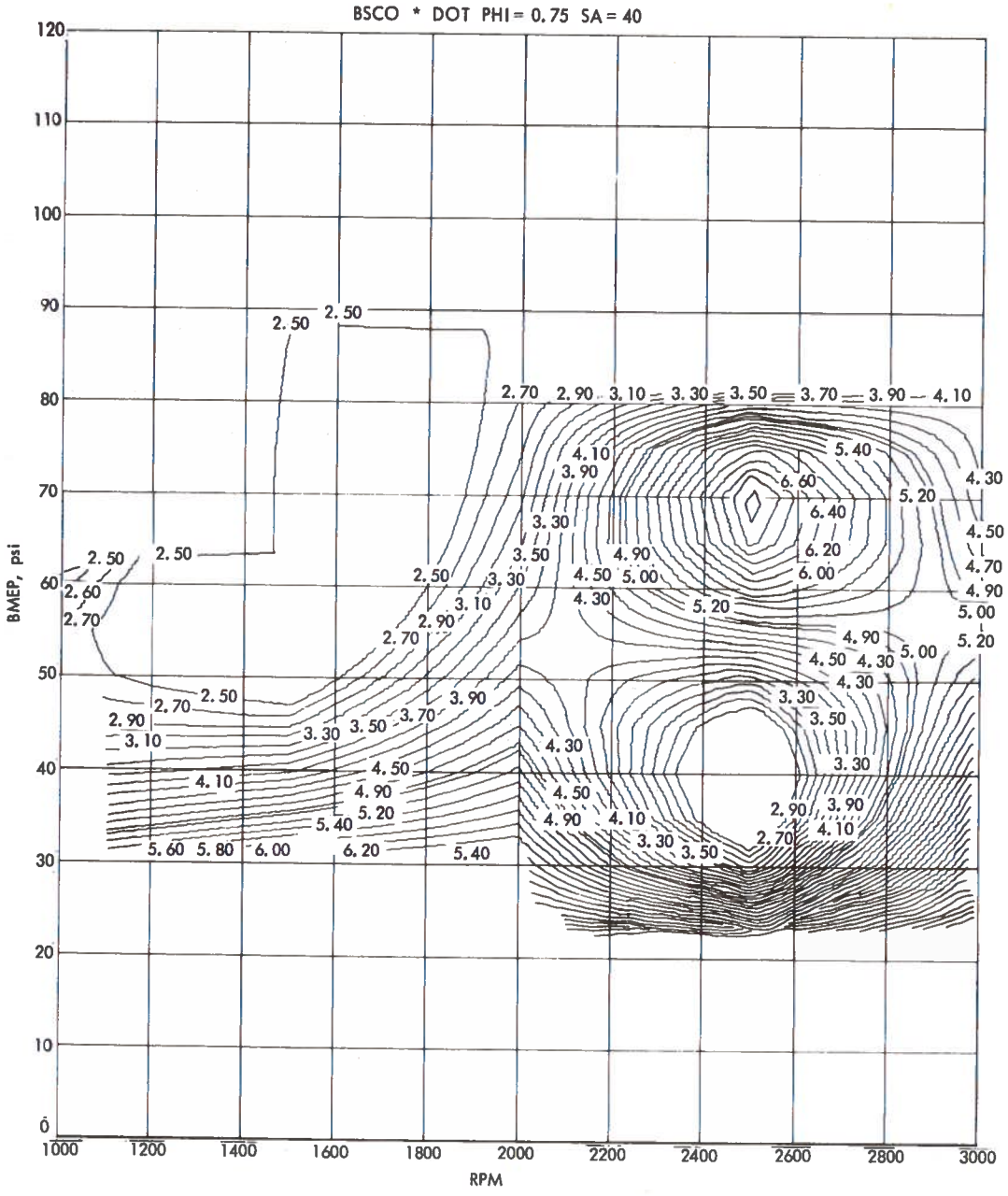

FIGURE E-52. BSCO CONTOUR MAP FOR LBEC-2 ENGINE
(Φ = .75, SA = 40)

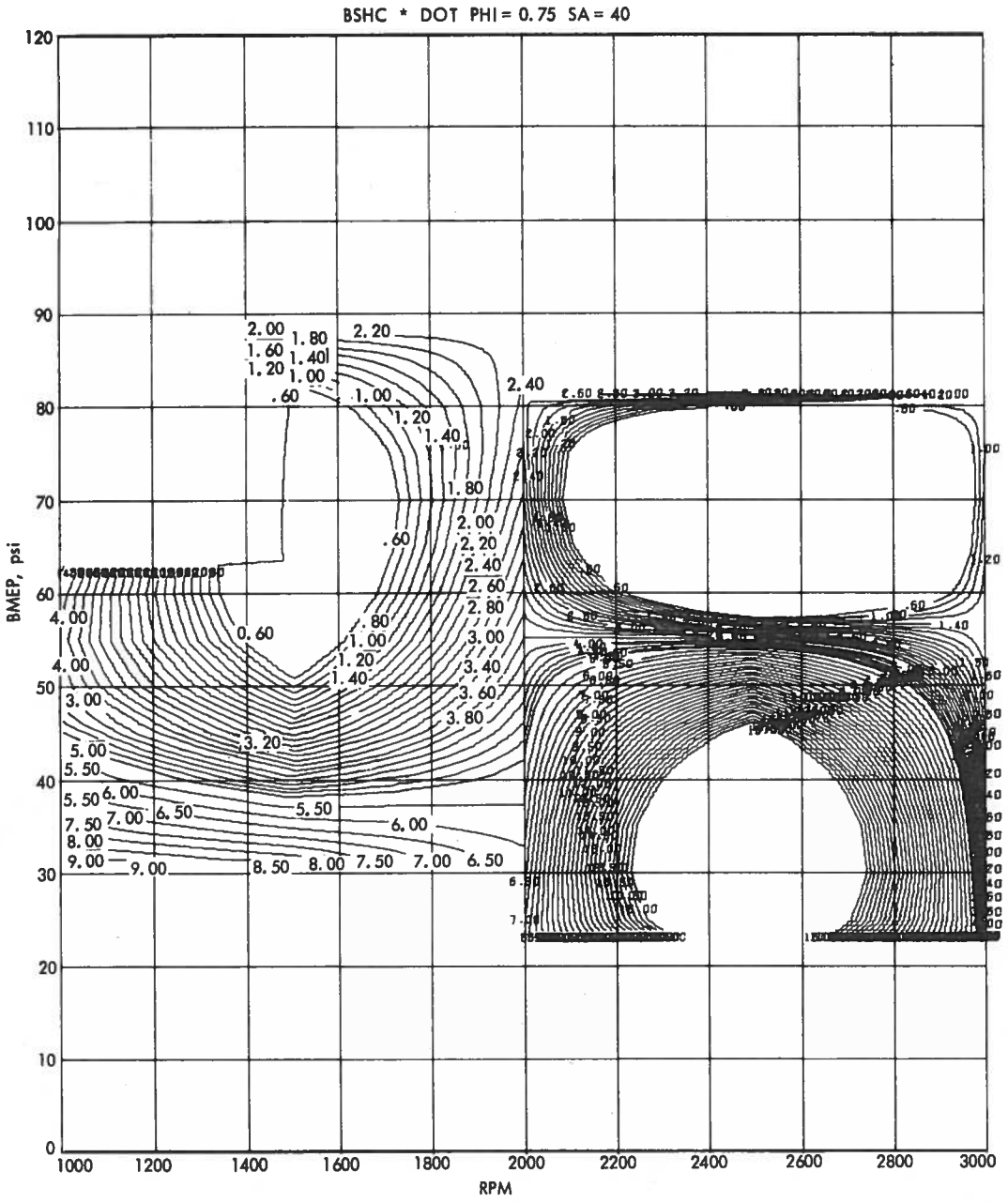

FIGURE E-53. BSHC CONTOUR MAP FOR LBEC-2 ENGINE
(Φ = .75, SA = 40)

APPENDIX F

PRESSURE-TIME DATA

FOR

LEAN BURN ENGINE CONFIGURATION No. 2

MBT SPARK TIMING

$\sigma_{P_{peak}} = 35.2$

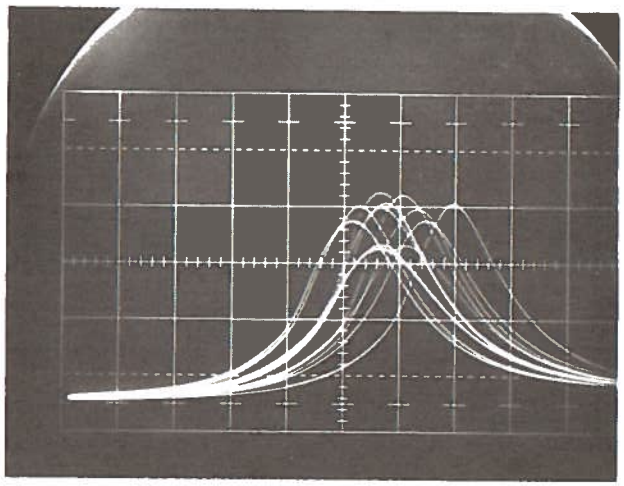

FIGURE F-1. PRESSURE-TIME DATA FOR LBEC-2
(N = 1973 RPM, BHP = 39.1, ϕ = 0.701)

MBT SPARK TIMING

$\sigma_{P_{peak}} = 15.8$

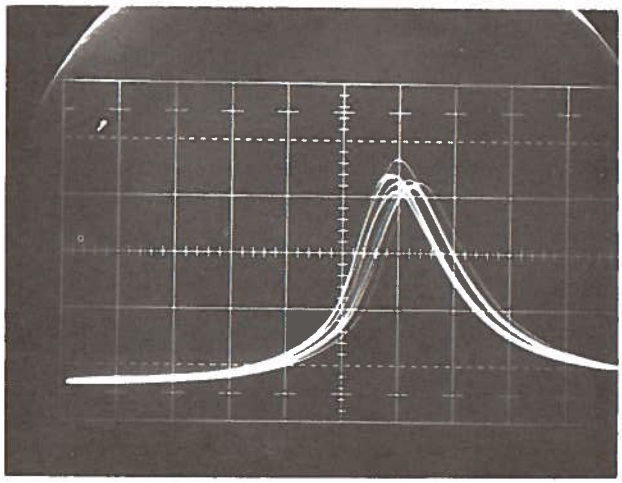

FIGURE F-2. PRESSURE-TIME DATA FOR LBEC-2
(N = 1975 RPM, BHP = 39.6, ϕ = 0.802)

MBT SPARK TIMING

$\sigma_{P_{peak}}$ = 14.75

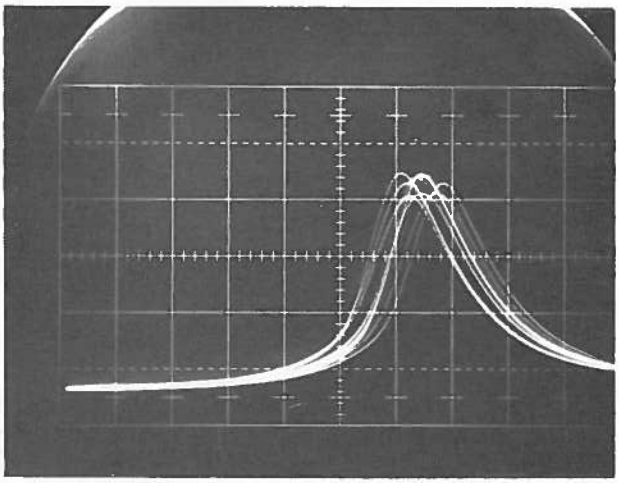

FIGURE F-3. PRESSURE-TIME DATA FOR LBEC-2
(N = 1986 RPM, BHP = 39.7, ϕ = 0.854)

MBT SPARK TIMING

$\sigma_{P_{peak}}$ = 11.75

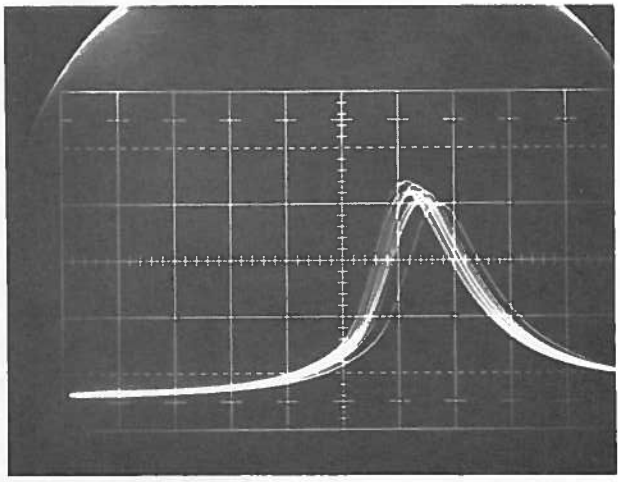

FIGURE F-4. PRESSURE-TIME DATA FOR LBEC-2
(N = 2008 RPM, BHP = 40.3, ϕ = 0.908)

MBT SPARK TIMING

$\sigma_{p_{peak}}$ = 16.05

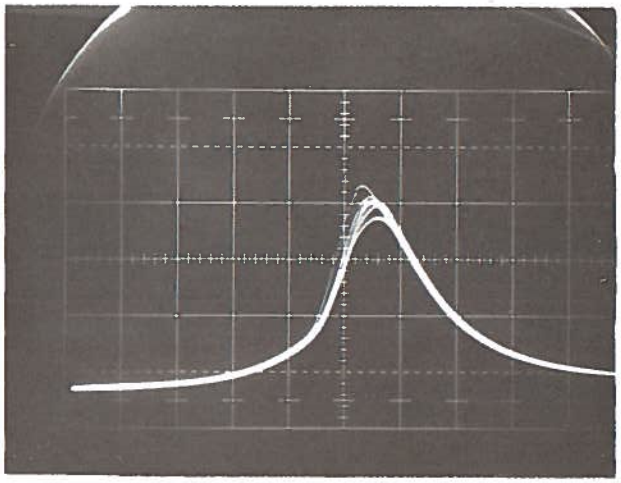

FIGURE F-5. PRESSURE-TIME DATA FOR LBEC-2
(N = 2004 RPM, BHP = 35.8, ϕ = 0.953)

MBT SPARK TIMING

$\sigma_{p_{peak}}$ = 10.15

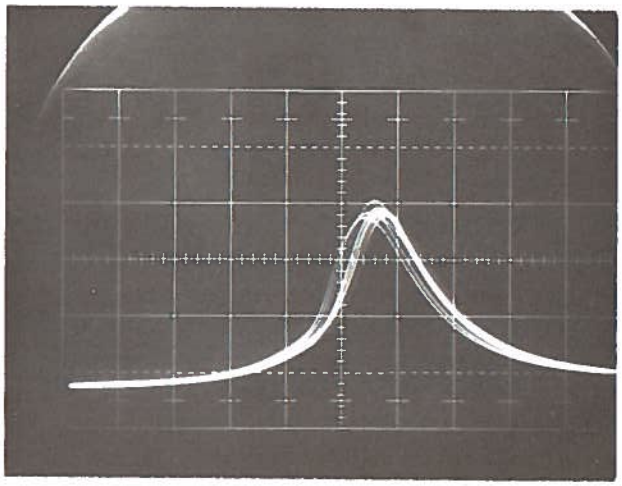

FIGURE F-6. PRESSURE-TIME DATA FOR LBEC-2
(N = 2034 RPM, BHP = 40.5, ϕ = 1.014)

MBT SPARK TIMING

$\sigma_{P_{peak}}$ = 27.45

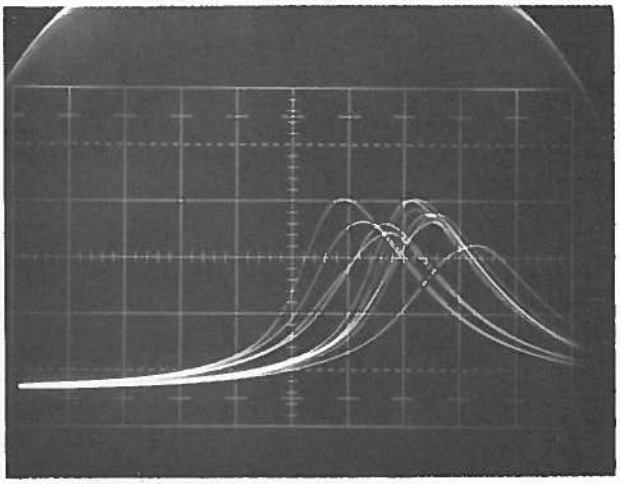

FIGURE F-7. PRESSURE-TIME DATA FOR LBEC-2
(N = 1474 RPM, BHP = 21.1, ϕ = 0.710)

MBT SPARK TIMING

$\sigma_{P_{peak}}$ = 35.65

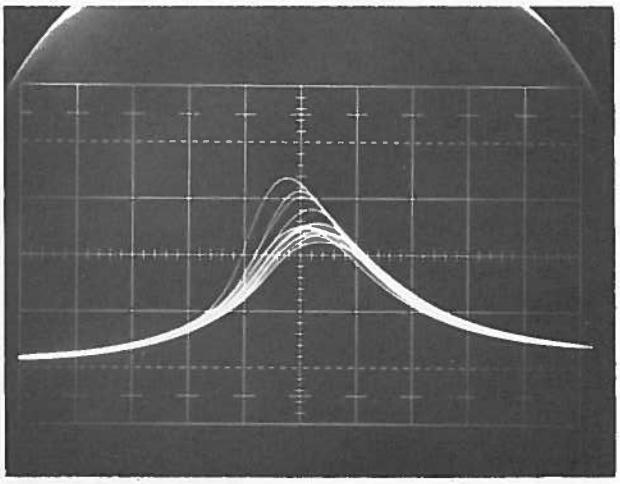

FIGURE F-8. PRESSURE-TIME DATA FOR LBEC-2
(N = 1485 RPM, BHP = 20.7, ϕ = 0.752)

MBT SPARK TIMING

$\sigma_{P_{peak}}$ = 19.05

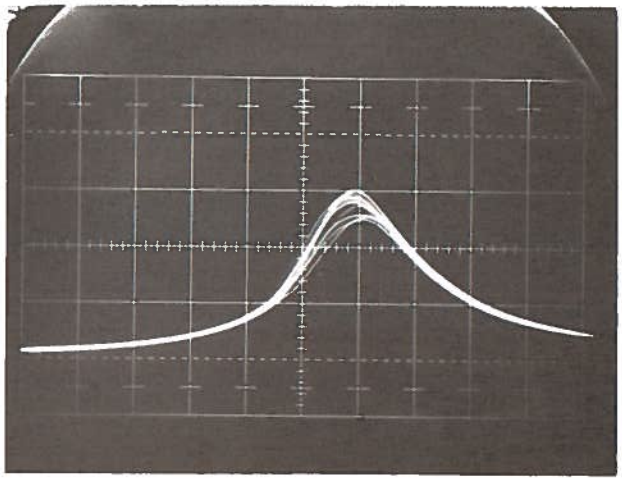

FIGURE F-9. PRESSURE-TIME DATA FOR LBEC-2
(N = 1492 RPM, BHP = 20.8, ϕ = 0.855)

MBT SPARK TIMING

$\sigma_{P_{peak}}$ = 19.85

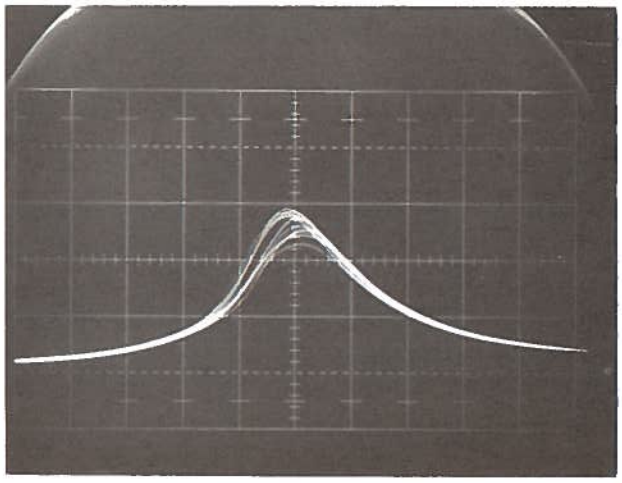

FIGURE F-10. PRESSURE-TIME DATA FOR LBEC-2
(N = 1505 RPM, BHP = 21.0, ϕ = 0.904)

MBT SPARK TIMING

$\sigma_{P_{peak}}$ = 11.1

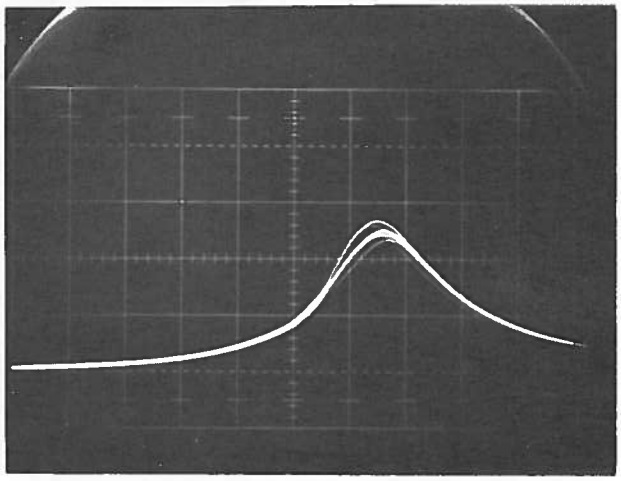

FIGURE F-11. PRESSURE-TIME DATA FOR LBEC-2
(N = 1497 RPM, BHP = 20.9, ϕ = 0.951)

MBT SPARK TIMING

$\sigma_{P_{peak}}$ = 14.05

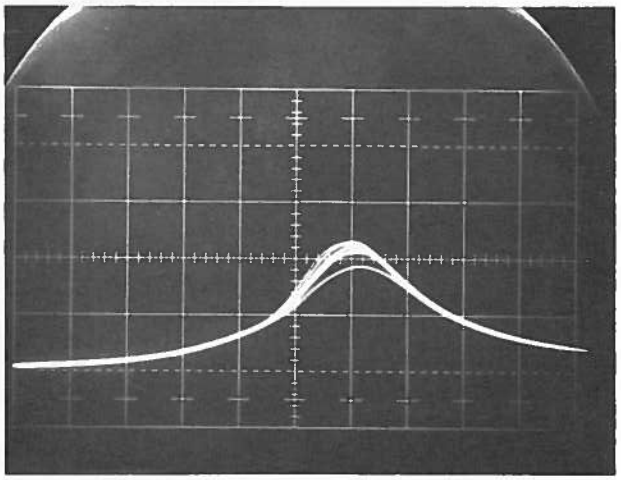

FIGURE F-12. PRESSURE-TIME DATA FOR LBEC-2
(N = 1493 RPM, BHP = 21.0, ϕ = 1.007)

MBT SPARK TIMING

$\sigma_{P_{peak}} = 15.6$

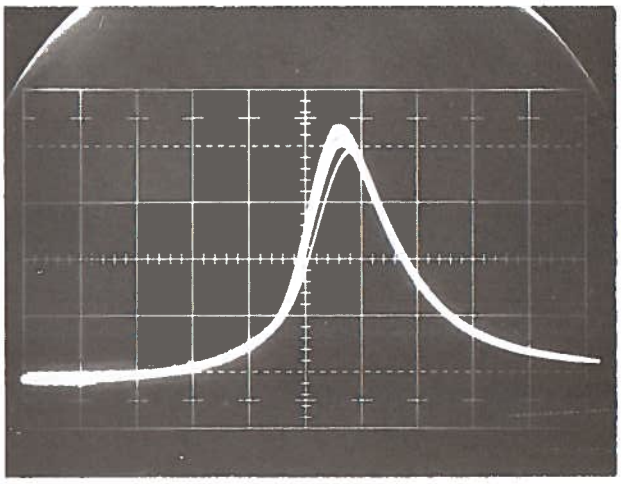

FIGURE F-13. PRESSURE-TIME DATA FOR LBEC-2
(N = 1995 RPM, BHP = 56.9, ϕ = 0.908)

MBT SPARK TIMING

$\sigma_{P_{peak}} = 20.75$

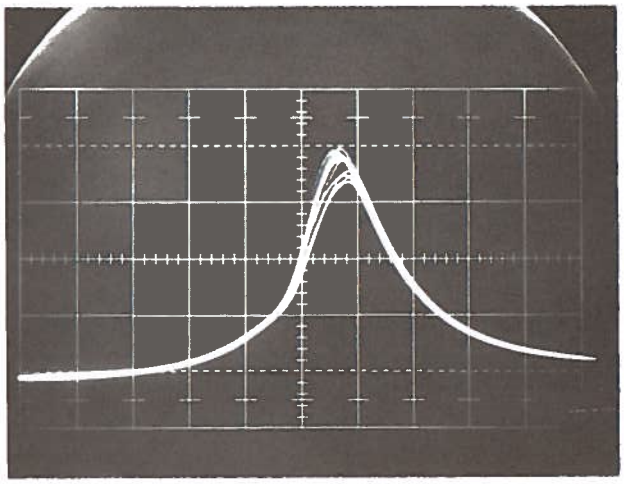

FIGURE F-14. PRESSURE-TIME DATA FOR LBEC-2
(N = 2002 RPM, BHP = 57.8, ϕ = 1.013)

MBT SPARK TIMING

$\sigma_{P_{peak}}$ = 38.5

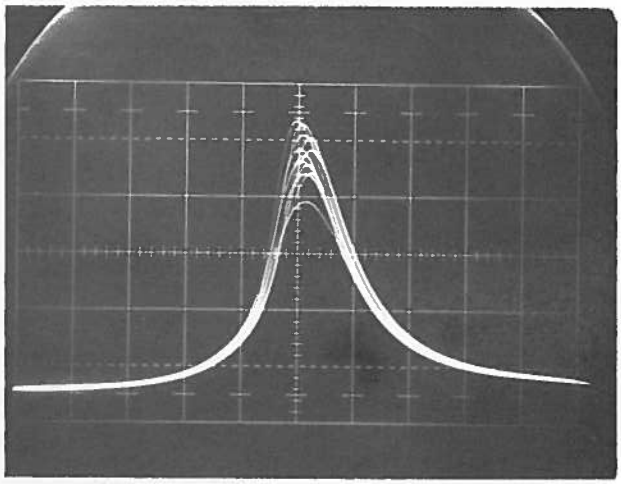

FIGURE F-15. PRESSURE-TIME DATA FOR LBEC-2
(N = 2477 RPM, BHP = 60.7, ϕ = 0.698)

MBT SPARK TIMING

$\sigma_{P_{peak}}$ = 28.45

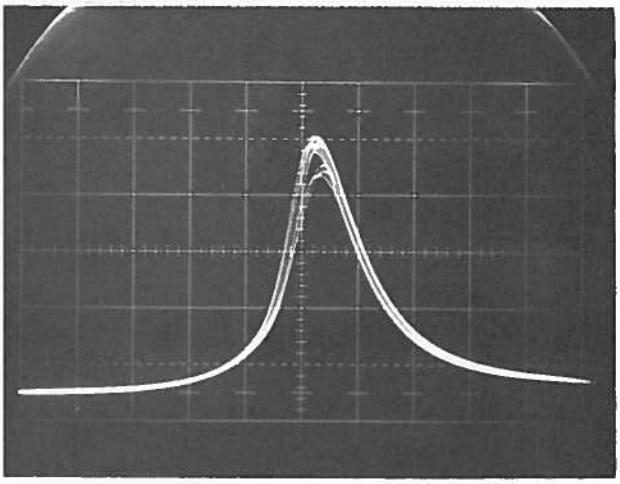

FIGURE F-16. PRESSURE-TIME DATA FOR LBEC-2
(N = 2518 RPM, BHP = 61.8, ϕ = 0.754)

MBT SPARK TIMING

$\sigma_{P_{peak}}$ = 14.25

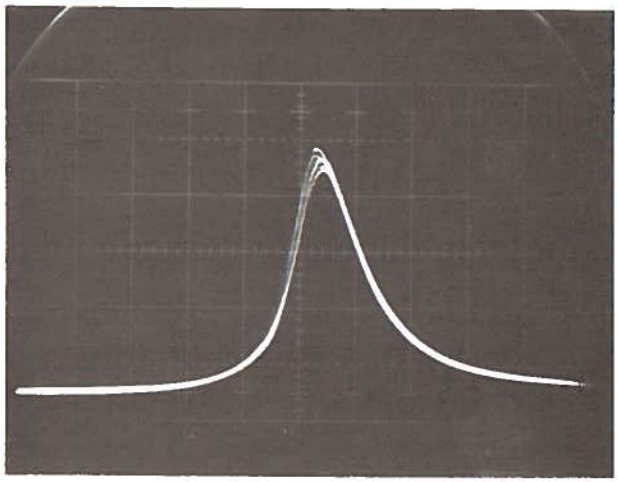

FIGURE F-17. PRESSURE-TIME DATA FOR LBEC-2
(N = 2520 RPM, BHP = 61.7, ϕ = 0.807)

MBT SPARK TIMING

$\sigma_{P_{peak}}$ = 27.9

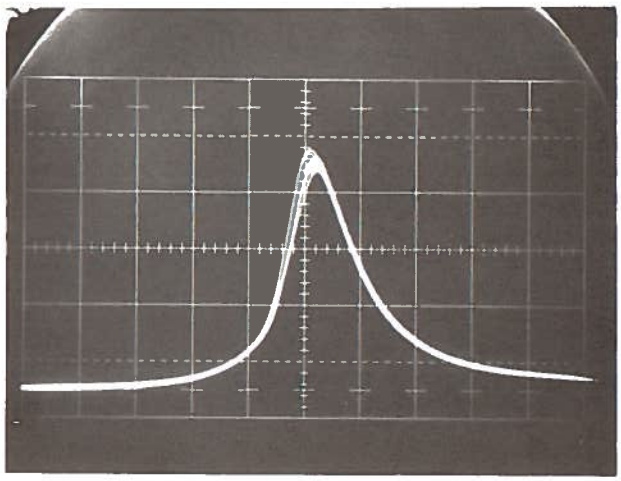

FIGURE F-18. PRESSURE-TIME DATA FOR LBEC-2
(N = 2508 RPM, BHP = 61.5, ϕ = 0.860)

MBT SPARK TIMING

$\sigma_{P_{peak}}$ = 18.3

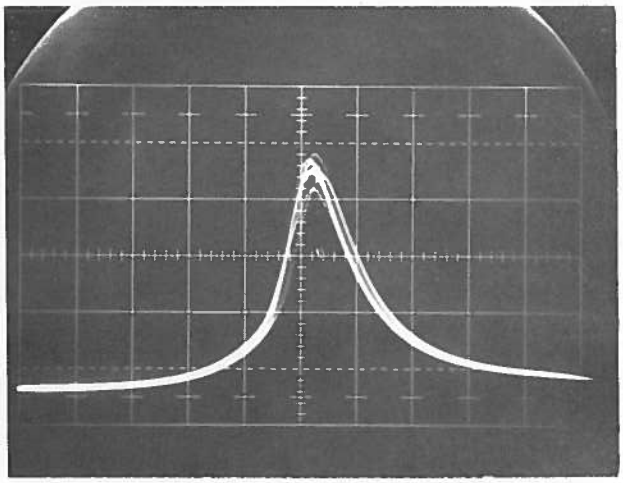

FIGURE F-19. PRESSURE-TIME DATA FOR LBEC-2
(N = 2537 RPM, BHP = 62.2, ϕ = 0.902)

MBT SPARK TIMING

$\sigma_{P_{peak}}$ = 17.45

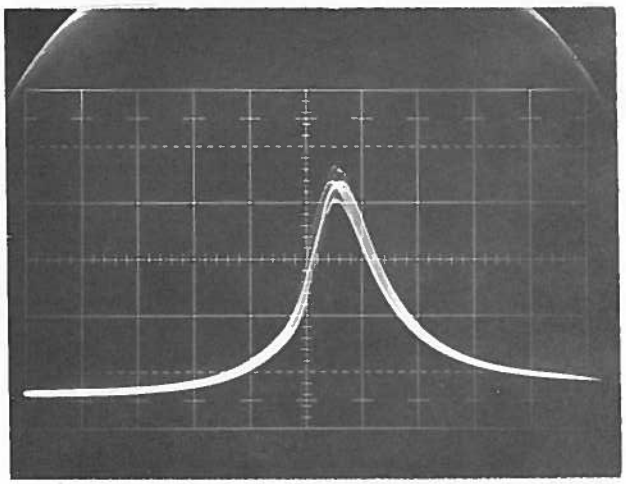

FIGURE F-20. PRESSURE-TIME DATA FOR LBEC-2
(N = 2507 RPM, BHP = 61.8, ϕ = 0.956)

MBT SPARK TIMING

$\sigma_{p_{peak}} = 14.35$

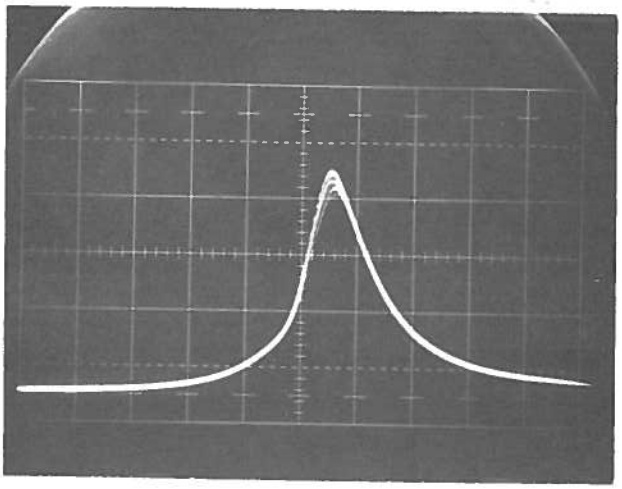

FIGURE F-21. PRESSURE-TIME DATA FOR LBEC-2
(N = 2499 RPM, BHP = 61.5, ϕ = 1.004)

APPENDIX G

INSTRUMENTATION

G.1 GENERAL DESCRIPTION

The instrumentation for the engine test program was based on equipment and techniques normally used at JPL. Three general areas required special development: a real-time data system program, special instruments for the engine testing, and emissions measurements. Other measurements such as pressures, temperatures and flows used routine technology.

The instrumentation capability is based on a digital data acquisition system that contains a capacity large enough to allow real-time output of not only engineering units data, but also key calculated parameters such as equivalence ratio and thermal efficiency. The real-time capability data permits engine operating conditions to be quickly set at the nominal value. The data acquisition time is very rapid. The recording time for over 100 channels is less than 20 seconds.

The instrumentation facility provides service to four separate test sites. Each site has its own set of transducers and unique instrumentation that is connected to the central area. The central area, shown in Figure G-1, includes the digital data system, analog recorders, and related instrumentation. Each site has one or more video displays that provide real-time data for the operator. Any of the 70 data channels may be displayed at the test site. In addition, some analog recording capability is provided at each test site for those parameters requiring continual monitoring. The video displays and analog recorders are shown in Figure G-2.

G.2 DIGITAL DATA SYSTEM

The Integrated Data Acquisition and Control (IDAC) data system was designed in 1966 as a general-purpose digital data system for JPL's propulsion test programs. Figures G-3 and G-4 show the system hardware and a block diagram of the system. The IDAC includes real-time data output and control

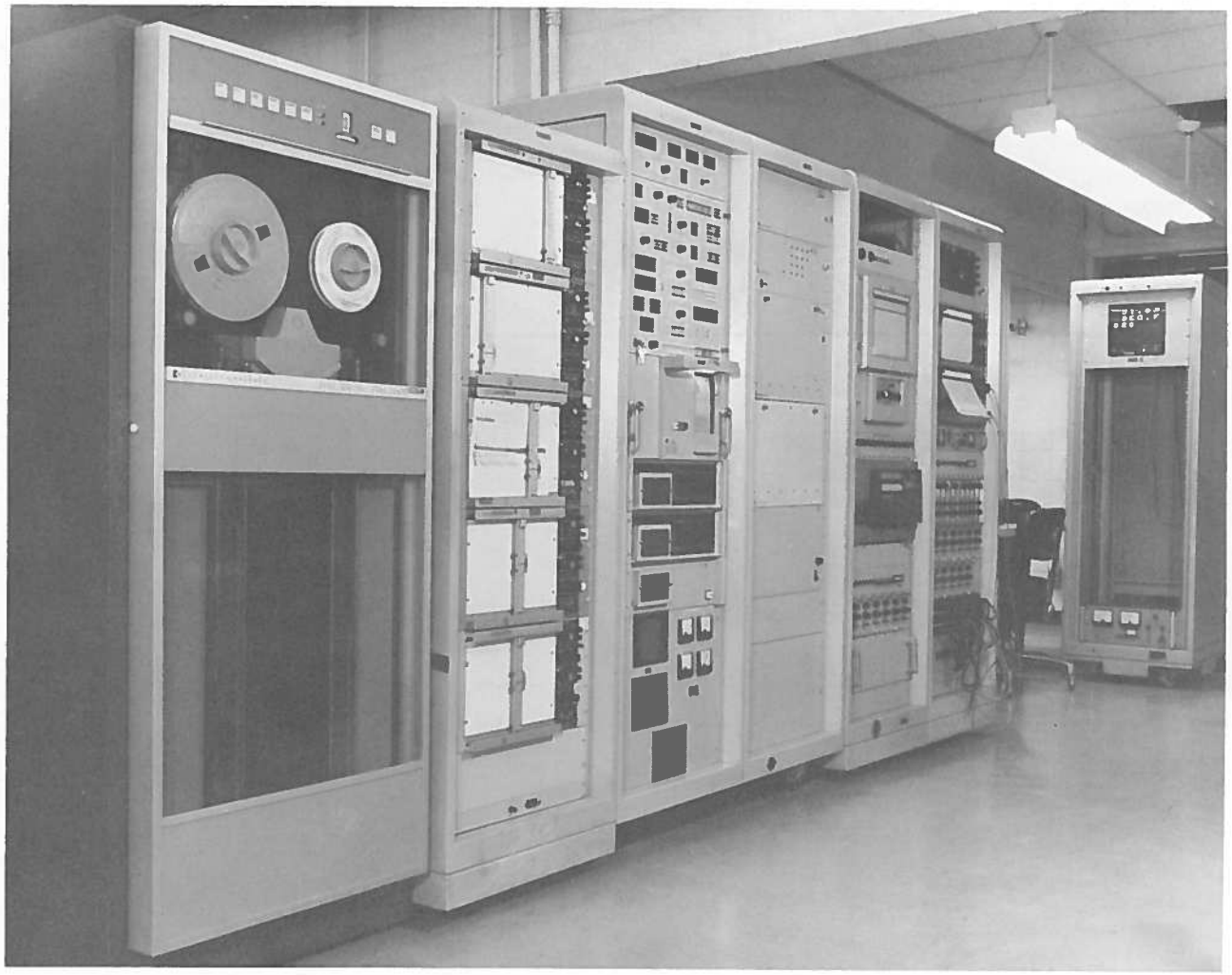

FIGURE G-1. CENTRAL INSTRUMENTATION AREA

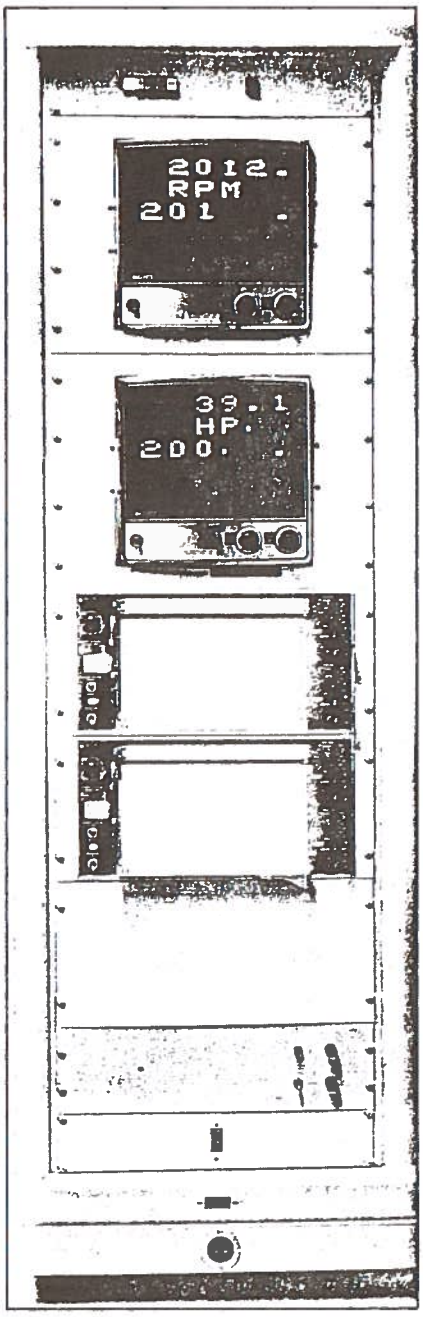

FIGURE G-2. LOCAL SITE VIDEO DISPLAYS AND ANALOG RECORDERS

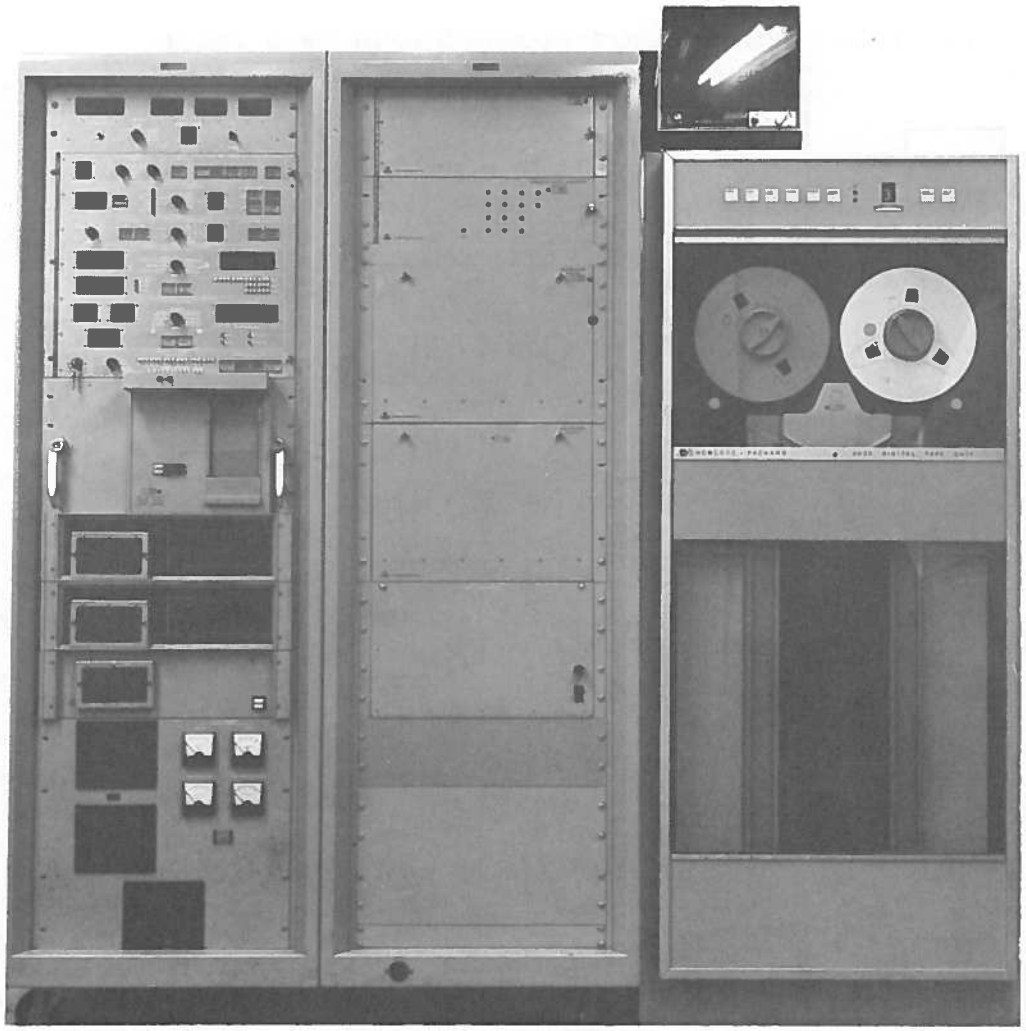

FIGURE G-3. INTEGRATED DATA ACQUISITION AND CONTROL (IDAC) DATA SYSTEM

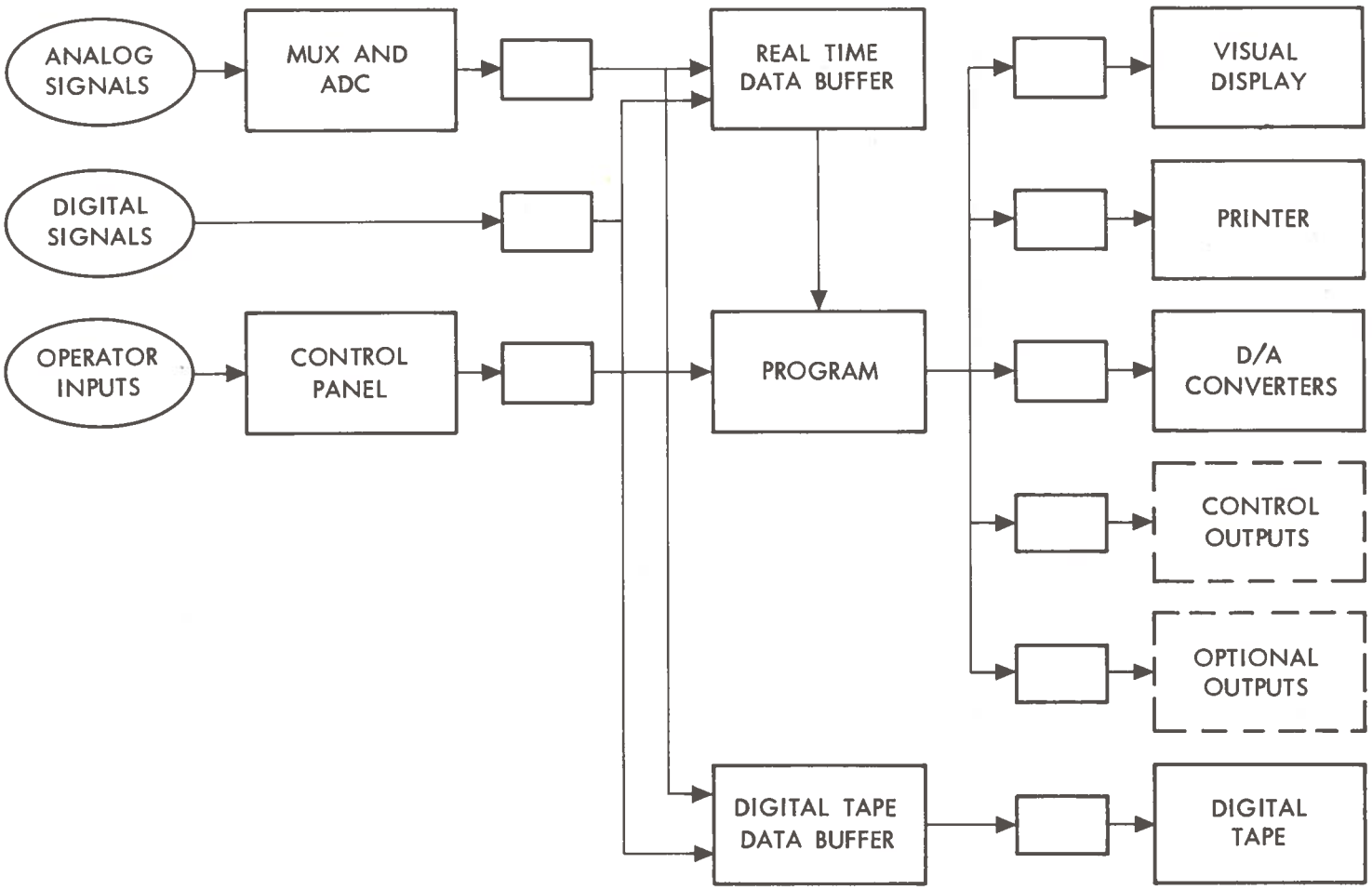

FIGURE G-4. BLOCK DIAGRAM OF IDAC DATA SYSTEM

capabilities. The analog input subsystem is typical of many digital systems: 500 channels, 14 bit ADC, scan rates to 10 kHz. addressable gain and channel selection, etc. The system includes an 8k, 18-bit memory and 75 in./sec digital, magnetic tape recorder. Real-time engineering unit output data is provided by a printed paper tape, eight video displays, and 16 digital-to-analog converters. The engineering units capability includes ranging and scale factors for all standard transducers, thermocouple linearization, and output with appropriate units. The system will limit check 64 data channels in real-time.

The IDAC also has a sophisticated digital data input capability in addition to the analog input subsystem. The digital input capabilities were used to acquire low frequency data from turbine type flowmeters to accept digital spark timing data, and to input codes defining the status of emission instruments.

The IDAC hardware and basic program was used for IC engine tests without modification. An additional program that provided the calculations unique to the engine test program was added. This program calculated key parameters that facilitated engine testing. These were:

1) Gasoline mass flow.
2) Air mass flow.
3) Equivalence ratio.
4) Thermal efficiency.
5) Emission instrument ranging and linearization.

Calculation errors for these parameters, independent of transducer errors, were on the order of 0.2%. Calculations for approximately 30 other parameters were also made and were available for real-time output. Data was updated at approximately 1/2 second intervals, which was more than adequate for the steady-state test conditions employed. A much faster sampling capability is inherent in the IDAC, but was not used for the testing described in this report.

G.3 SPECIAL INSTRUMENTATION

Two unique capabilities were employed for the testing described in other sections of the report. These were the capability to measure spark timing and individual cylinder pressure.

G.3.1 Cylinder Pressure-Time Capability

A high-response pressure measurement system was implemented on the V-8 engine to obtain individual cylinder pressure-time data. Pressure taps were drilled directly through the engine heads adjacent to the spark plug locations. A piezoelectric pressure transducer was mounted as closely as possible to the cylinder head. Shock tube tests verified that this pressure measurement had adequate frequency response as shown in Figure G-5.

The pressure transducer signal was converted to a digital value at 1-deg crankshaft intervals during the compression and power strokes. In order to attain accurate digital values at precise 1-deg intervals, a timing disc with holes located every 10 deg was attached to the crankshaft as shown in Figure G-6. Electrical pulses derived from these holes were used as inputs to a phase-locked loop circuit. This circuit provided an output pulse at 1-deg intervals with a maximum of ±0.1 deg deviation from the nominal value. These 1-deg pulses were used as control signals to a circuit that held the value of the analog combustion pressure signal constant from the instant of the 1-deg pulse until the conversion to a digital value was completed. A digital value proportional to the combustion pressure with 0.1% resolution was thus obtained at precise 1-deg crankshaft intervals.

The 360 pressure measurements for one cycle were temporarily stored, then transferred to a permanent location through an averaging program. The time required for the averaging computation dictated that alternate cycles were measured. The acquisition-averaging sequence was continued until averaged data for a specified number of cycles was stored in the permanent

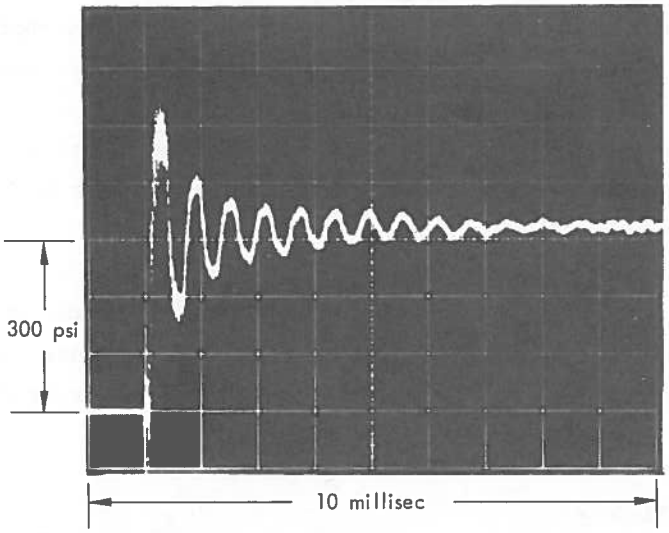

RISETIME: 300 psi IN 100 μsec

NATURAL FREQUENCY: 1.7 kHz

FIGURE G-5. TRANSDUCER RESPONSE FROM SHOCK TUBE TESTS

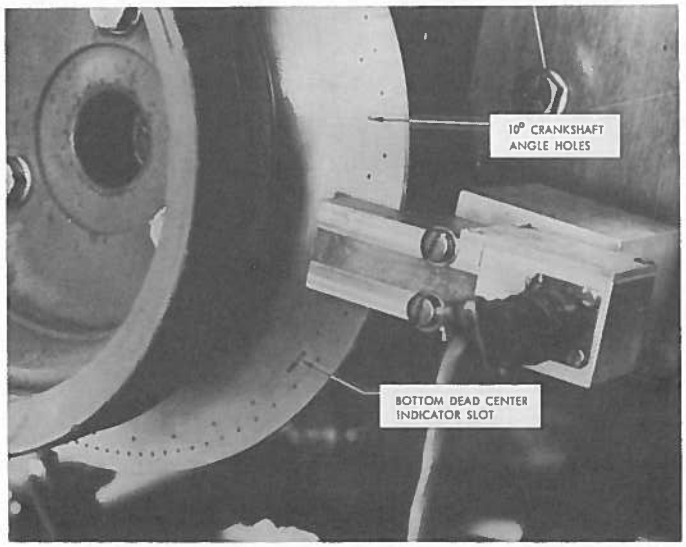

FIGURE G-6. PHOTOGRAPH OF TIMING DISC MOUNTED ON ENGINE

location. The averaged motoring and firing data were based on 10 and 100 cycles respectively. Motoring pressure data were obtained by electrically shorting the spark to the cylinder whose pressure was being monitored while maintaining engine RPM and load with the remaining 7 cylinders. The average motoring data, the average firing data, and the difference between these two conditions were then plotted versus crankshaft angle. A mark defining the spark time within ±0.2 deg was also included.

To obtain an indication of cycle-to-cycle pressure variations, photographs were made of multiple pressure traces using a storage oscilloscope. Approximately 10 successive cycles were recorded for both the motoring and firing modes.

G.3.2 Spark Timing

Pulses at 10° crankshaft intervals are derived from a disc attached to the crankshaft. These pulses are imput to an electronic phase locked loop circuit. This loop tracks the 10° pulses and provides an output frequency 100 times the input frequency, i.e., 0.1° resolution. Firing of the number 1 spark plug generates a signal that passes the 0.1° pulses to a counter. The counter is turned off at TDC, thus providing a count equal to the spark timing with 0.1° resolution. The logic includes the capability to measure spark timing after TDC. The sparking timing error is less than ±0.2° at steady-state engine speeds. The counter output is available in BCD form and is recorded by IDAC via a digital input channel.

G.4 CENTRAL INSTRUMENTATION EQUIPMENT

The central instrumentation includes equipment typically used in JPL test facilities. A patchboard permits typical data channels from the four test sites to share this equipment and the digital data acquisition system. The exhaust emission instruments were also shared by all test sites.

G. 4. 1 Typical Data Channels

Data channels for all standard measurements, such as temperatures, pressures and liquid flows, used standard JPL instrumentation techniques. Data channels with unusual characteristics are briefly discussed here.

G. 4. 1. 1 Gasoline Flow. JPL has typically used turbine flowmeters for liquid flows, and the IDAC system digital input capability was designed specifically to accept the frequency output of these flowmeters. Turbine flowmeters normally have a 10:1 dynamic flow range, so three flowmeters were required to cover the 0. 001 gpm to 0. 5 gpm range. The lowest flowrate, which can be approximated by one drop per second, is measured by a flowmeter with a paddle wheel type rotor.

The gasoline flow was routed to the appropriate flowmeter by a solenoid valve controlled from the test site console. The flowmeter range overlapped approximately 20%, so the gasoline flow path was arranged to permit flow in the range common to two flowmeters to be passed through both the flowmeters. This permitted checks on the flowmeter calibrations.

The IDAC accepted the flowmeter frequency, gasoline temperature, gasoline pressure, and flowmeter codes. The latter was used to access the flowmeter calibration constants for the active flowmeter; a quadratic equation converted the frequency to volume flow. Real-time data, corrected for temperature effects, was output in units of lbm/hours.

G. 4. 1. 2 Gaseous Flows. Gaseous flows were measured by a laminar flow transducer; the differential pressure across the flowmeter is linearly proportional to the actual volume flow through the flowmeter. To provide mass flow data, absolute pressure and temperature measurements are also required. The differential pressure transducer is purposely installed at an angle that reduces to a negligible value the zero shift resulting from the absolute pressure.

G. 4. 1. 3 Exhaust Emissions Measurements. Exhaust emissions are measured by an emission bench, shown in Figure G-7, that utilizes instruments in general acceptance by the automotive industry. A description of the individual instruments used is given in Table G-1.

TABLE G-1. EMISSION INSTRUMENTS

Parameters	Measurement Instrument Manufacturer	Model	Range	
			Highest	Lowest
HC	Horiba	FID-2	5 k ppm	10 ppm
NO_x	Thermal Electron Corp.	12A	10 k ppm	1 ppm
CO-High	Horiba	A1A-21	10%	5%
CO-Low	Horiba	A1A-21	1 k ppm	250 ppm
CO_2	Horiba	A1A-21	20%	10%
O_2	Beckman	778	25%	-

The engine exhaust gas sample was continuously filtered and passed through moisture condensing coils and then distributed to each of the flow bench analyzer instruments. Calibration of each analyzer was accomplished daily using the appropriate calibration gases.

Initial difficulties with calibration gases from several suppliers, particularly NO_x, were resolved by comparing JPL's calibration gases to standard gases at the GM Proving Ground's Van Nuys facility, whose emission measurements are compared to those accepted by the automotive industry at periodic intervals.

The CO_2 and CO measurements were made using the principle of infrared absorption. Two infrared beams from dual collimated light sources pass

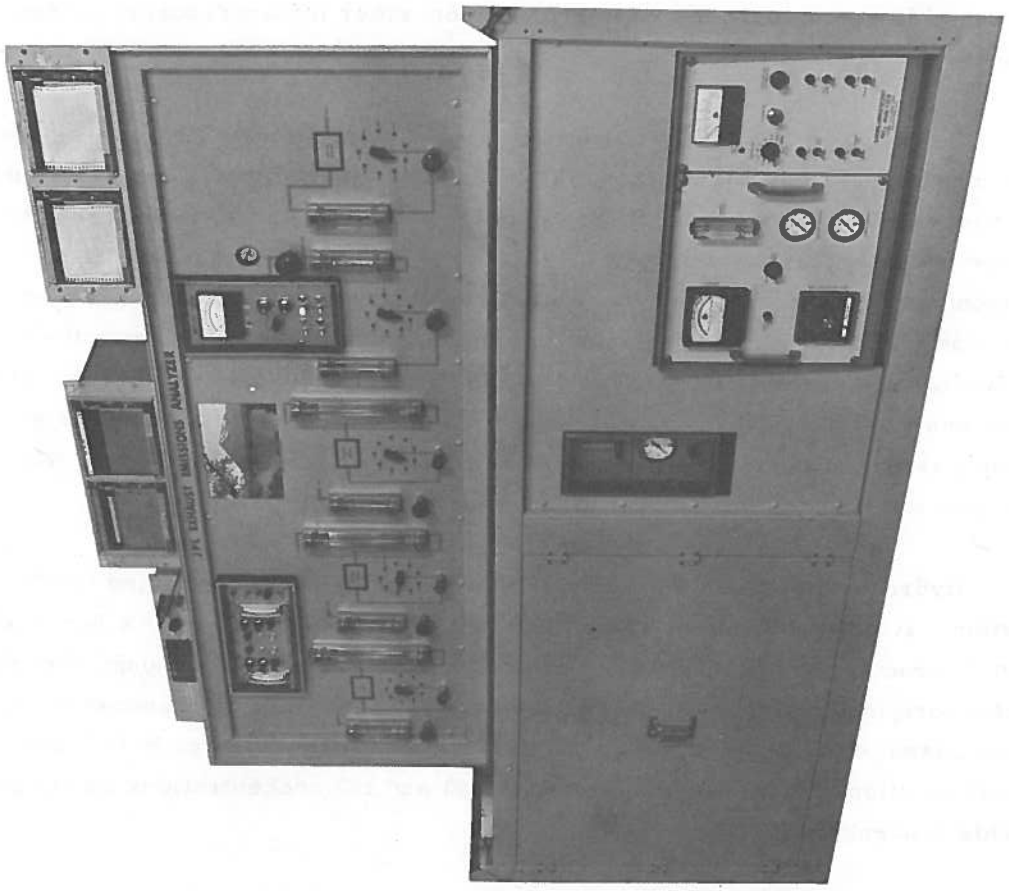

FIGURE G-7. EMISSION BENCH

through a reference and a sample cell and are interrupted simultaneously by a rotating optical chopper and then directed to a detector. The portion of the infrared radiation absorbed is proportional to the concentration of the component of interest in the cell. The non-absorbed portion of the infrared radiation passed through the sample cell is sensed by the detector and compared to the infrared energy passing through the reference cell. This difference is converted to an electrical signal by the detector sensitized to the given component of interest minimize interference from other infrared-absorbing components in the sample stream.

To measure NO concentrations, the gas sample to be analyzed was blended with ozone (O_3) in a flow reactor. The resulting chemiluminescent reaction is monitored through an optical filter by a high sensitivity photomultiplier positioned at one end of the reactor. The filter photomultiplier combination responds to light in a narrow wave length band unique to the above reaction. The flow parameters were adjusted in such a way that the output from the photomultiplier was linearly proportional to the NO concentration. The same instrument analyzes for NO_x (i.e., mixture of NO and NO_2). In this mode the gas sample is first passed through a thermal reactor to convert the NO_2 to NO. The gas sample then follows the process described above.

Hydrocarbons were measured with a flame ionization detection (FID) system. A gas sample containing HC's will, when passed through a hydrogen flame, produce an ionization current proportional to the total amount of carbon atoms (originally present as HC) in the sample. There is no response to inorganic gases (other than oxygen) such as CO, CO_2, NO, NO_2, or H_2O. The linear relationship between the output signal and HC concentrations exists over a wide concentration range.

Each emission instrument was modified so that the instrument output included a signal indicating the full scale range in use. This range information permitted real-time emissions data from the IDAC. The output of the CO and CO_2 instruments are non-linear; therefore, a quadratic fit was used and matched the calibration curve to within ±1%. The other emissions instruments were sufficiently linear that a straight line approximation to the calibration was sufficient.

G.5 MEASUREMENT ACCURACY

The initial setup for each data channel was based on standard JPL transducer calibration techniques. Data taken during initial tests were examined to verify the measurement for all key channels. Either redundant measurements or comparison of interrelated calculated parameters, which permitted individual measurements to be checked, was used for the initial verification. Individual channels remained undisturbed for the entire test series except for modifications required to meet the requirements of various test configurations.

Tests to define measurement accuracy of key parameters were conducted near the end of the engine test program. The measurement accuracy tests did not provide adequate data for a rigorous error analysis since the time required would have significantly reduced engine test time. In general, the measurement tests obtained enough data to provide reasonable accuracy specifications when reasonable assumptions, based on past JPL measurement techniques, were included in the error calculations.

G.5.1 Procedure and Error Summary

Approximately 50 data channels provided the basic data for the V-8 engine tests. These channels were converted to engineering units for real-time display and printout. Approximately 15 of these channels were used as source data for calculations that provided the primary calculated parameters, such as horsepower, thermal efficiency, and equivalence ratio, for the engine test program. The measurement accuracy tests defined the performance of the particular source channels that were used for the calculations; only limited checks of other channels were conducted since their characteristics were essentially identical to the source channels. Source channel performance was then used to define accuracy of the calculated channels.

G.5.2 Source Channel Errors

Measurement performance of the source channels was defined with three different techniques:

1) End-to-end Calibrations -- Known physical quantities were used as inputs to the data channels used for the test data. Digital data from IDAC was compared to the known physical inputs, thus verifying performance of the entire data channel. This technique was used for pressure and temperature data.
2) Laboratory Calibration -- Laboratory facilities were used to calibrate gaseous flow transducers since no physical inputs suitable for on-site calibrations were available. The remaining components of the data channel were verified either by substituting a precision voltage for the transducer's electrical output or comparing individual elements of the data channel to a known electrical standard.
3) On-site Derived Calibrations -- Measurement of time interval, total counts, fluid temperature and either fluid volume or weight was used to verify gasoline flow measurements. This technique used all components (lines, pressure system, valves, etc.) of the normal test system to simulate the actual test conditions as closely as possible.

The equipment used to generate the physical inputs for the end-to-end checks was calibrated by the JPL Standards Lab prior to the checks. The deviation between the JPL Standards Lab and the equipment used for end-to-end checks is defined in Table G-2.

Table G-3 summarizes the results of the measurement performance tests for the source channels.

G.5.3 Calculated Channel Errors

Errors for calculated data are summarized in Table G-4. These errors are determined by the source channel errors and the equation for each calculation.

TABLE G-2. ACCURACY OF EQUIPMENT USED FOR END-TO-END SOURCE CHANNEL CALIBRATIONS

Equipment	Parameter Checked	JPL Standards Lab Certification	Deviation Between Equipment and Stds. Lab
Dead Weight Tester	Gage Pressure	± .005% of F. S.	- .15% at 500 psi
Precision Manometer	Differential Pressure	± .14%	
Temperature Bath	Temperature	± .018° F	(1) .09° F Linearity ± .018° F Stability
Digital Voltmeter	Voltage	± 10 PPM	(1) ± .004% Reading + .002% F. S.

(1) Instruments were within the manufacturer's specification that is stated in the Table.

TABLE G-3. MEASUREMENT PERFORMANCE OF TYPICAL CHANNELS

Parameter	Verification Method	Verification Equipment	Transducer Type	Typical Results of Performance Verification		
				Verification Range	Error	Repeatability
Gage pressure	End-to-end	Dead weight tester	Strain gage	0-600 psig	± 0.4%	± 0.2%
Absolute pressure	End-to-end	Mercury manometer	Strain gage	10-50 psia	± 0.5%	± 0.2%
Differential pressure	End-to-end	Precision manometer	Strain gage	0-0.2 psid	- 1.4%	± 0.3%
Temperature	End-to-end	Water bath, quartz electronic thermometer	Thermo-couple Type E	60-80° F	- 0.4° F	± 0.2° F
Gaseous volume flow	Lab calibra-tion	-	Laminar flow	Various	± 1%	± 0.5%
Liquid volume flow	On-site calib.	Stopwatch, volume, counter	Turbine flow-meter	0-0.1 gpm	± 1.3%	± 1%
Engine torque	End-to-end	Dead weight, moment arm	Gage pressure transducer, moment arm	0-150 #ft	- 2%	± 0.5%
IDAC data system	Lab calibra-tion	Digital voltmeter	Multiplexer & ADC	0-100 mv (full scale)	± 0.05% (worst case)	± 0.02%

TABLE G-4. PRIMARY REAL-TIME CALCULATED PARAMETER ERROR

Parameter	Error
Engine HP	- 2.0%
Gasoline mass flow	± 1.3%
Carburetor air mass flow	- 1.6%
Equivalence ratio	± 2.8%
Thermal efficiency	± 0.3%

The equation was differentiated, then evaluated at typical operating conditions for the course channel errors to obtain the stated error value.

A baseline test condition was periodically run with the lean burn engine to determine the repeatability of performance and emissions measurements and thereby establish a level of confidence for the test engine and data acquisition system. The run condition selected was 2000-RPM, 40-BHP (29.8-kW), level-road-load power, an equivalence ratio of 0.85, and a spark advance of 44° BTDC. A statistical evaluation of the test data from 8 tests yielded the results shown in Table G-5. Based on a 95% confidence level, the percent deviation in indicated thermal efficiency is ±1%, while the corresponding deviation in the exhaust emissions data is about 15%. These variations are due to a combination of engine setting variations and measurements.

G.5.4 Measurement Accuracy Tests

This discussion is limited to comments on significant errors disclosed by the measurement accuracy tests.

TABLE G-5. STATISTICAL ANALYSIS OF BASELINE DATA

Parameter	Confidence Range at 95% Probability	Percent Deviation at 95% Probability $1.86 / \bar{x} \times 100$
RPM	1985 - 2039	1.35
BMEP, psi	44.8 - 45.7	1.03
ϕ	0.848 - 0.854	0.37
η_{t_I}	0.359 - 0.366	0.95
NO_x, ppm	2648 - 3628	15.6
HC, ppm	1162 - 1434	14.5
CO, %	0.077 - 0.103	14.5

G.5.4.1 Torque. The engine dynamometer measures the reaction force by converting the force to a pressure by means of a piston and cylinder mechanism. This pressure was then measured by a strain gage pressure transducer. The calibrated dead weight tester was connected to the pressure transducer to define characteristics of the pressure measurement. Results showed the measurement error to be primarily caused by hysteresis, but within a nominal ±0.5% up to the maximum pressure of 300 psi used for this test.

The pressure check did not include dynamometer errors which could be caused by:

1) Bearing friction.
2) Piston cylinder seal friction.
3) Piston diameter errors.
4) Moment arm length error.

The first two would cause hysteresis, the latter two scale factor errors. These possible errors were defined by a torque check.

A moment arm with a length of 24.04" ± .01" was installed on the dynamometer housing. Calibrated weights, known to ± .02%, were hung from the moment arm. The results showed a large (8%) hysteresis loop but reasonable (-2%) scale factor error up to approximately 2/3 full scale. This test was conducted with the engine off, but included firm tapping of the dynometer frame before data was taken to minimize friction. The test was repeated with the engine running at 1750 to 2000 rpm to investigate the effort of engine vibration. Two tests were conducted, 2nd showed a significant reduction in the hysteresis loop. The agreement between the two tests indicates that the curves provide a good definition of torque measurement errors, and that errors were within +0 to -2% up to 200 # ft torque when torque was increased. This range included all data taken for the V-8 tests.

G.5.4.2 Differential Pressure. The gaseous flow measurements consisted of a differential pressure measurement across a laminar flow element. The low-range (0.3 psid) differential pressure transducers were initially calibrated in the JPL pressure calibration laboratory. The end-to-end measurement accuracy checks disclosed an error of - 1.42% in the calibration for the carburetor air flow differential pressure measurement. This error was traced to a calibration laboratory procedure used for this particular pressure range. The differential pressure measurements were verified by paralleling a precision manometer with the differential pressure transducer during actual engine operation. The pressure indicated by the manometer was compared to the IDAC engineering units data to provide an end-to-end check of this measurement. The precision manometer is also used as a laboratory calibration device. The manometer error is ±0.14% at the ranges used for the verification. Density of the fluid in the manometer was checked to within 0.1% during the investigation; the density agreed with published data within readability limot of the temperature vs. density graph, which was approximately 0.05%.

G. 5. 4. 3 Gaseous Flow Transducers. Calibrations of the gaseous flow transducers were performed by an outside vendor that complies with MIL-C-45662A, the accepted specification for this type of calibration. The vendor's traceability to NBS is verified at 6 month intervals by DCASR/LA metrology specialists. The vendor's stated accuracy is ±0. 5%.

APPENDIX H

REPORT OF INVENTIONS

A diligent review of the work performed under this contract has revealed no innovation, discovery, improvement or invention of a patentable nature.

NASA — JPL — Coml., L.A., Calif.